

AN ABSTRACT OF THE THESIS OF

Vi-Vie Ng for the degree of Master of Science in Electrical and Computer Engineering
presented on March 18, 2010.

Title: Integration of Vapor-Solid Grown ZnO Nanowires Through Dielectrophoresis.

Abstract approved:

John F. Conley, Jr.

Work on individually constructed devices has demonstrated that nanowires (NWs) offer great promise for applications such as sensing and optoelectronics. Despite this work, reliable large scale alignment and integration of these individual nanostructures into a lithographically defined process remains a challenge.

Dielectrophoresis (DEP) is a promising alignment method in which a nonuniform electric field is used to exert force on and manipulate NWs in solution. DEP offers the possibility of rapid, large area room-temperature assembly of NWs across opposing electrodes. DEP structures were fabricated on Si substrates and

consisted of pairs of parallel Al electrodes on a 100nm insulating SiO₂ film. ZnO NWs were suspended in isopropyl alcohol (IPA) and flowed across the electrodes.

Alignment yield and angle of alignment were investigated as a function voltage and frequency. A method to remove excess nanowires through frequency tuning and IPA flushing is also investigated. The electrical properties of the formed ZnO NW devices will be reported.

©Copyright by Vi-Vie Ng

March 18, 2010

All Rights Reserved

Integration of Vapor-Solid Grown ZnO Nanowires Through Dielectrophoresis

by

Vi-Vie Ng

A THESIS

submitted to

Oregon State University

in partial fulfillment of

the requirements for the

degree of

Master of Science

Presented March 18, 2010

Commencement June 2010

Master of Science thesis of Vi-Vie Ng presented on March 18, 2010

APPROVED:

Major Professor, representing Electrical and Computer Engineering

Director of the School of Electrical Engineering and Computer Science

Dean of the Graduate School

I understand that my thesis will become part of the permanent collection of Oregon State University libraries. My signature below authorizes release of my thesis to any reader upon request.

Vi-Vie Ng, Author

ACKNOWLEDGEMENTS

I would like to thank Dr. Chien-Chih Huang for the countless help and support that he has provided since the beginning of this research. The great mentorship that he offered has helped me tremendously in making this thesis a success.

Also, I would like to thank Josh Triska for his willingness to build the setup used for the dielectrophoresis experiment as well as his inputs on various discussions concerning this research. To Santosh Murali, thank you for calculating some of the parameters used in this thesis. Not forgetting the rest of the team members, thank you all for the help you have given.

I would especially like to thank my family and friends who have given great encouragement throughout this journey. Thank you very much for believing in my ability.

Finally, this research would not have been possible without Dr. Conley. Thank you for providing inputs on various research methods and the very thorough review of this thesis.

TABLE OF CONTENTS

	<u>Page</u>
1. INTRODUCTION	1
2. LITERATURE REVIEW	4
2.1 Nanowire Synthesis Methods.....	4
2.1.1 Vapor-Solid	5
2.1.2 Vapor-Liquid-Solid	6
2.1.3 Hydrothermal	8
2.2 Nanowire Characterization.....	9
2.2.1 Physical Properties	9
2.2.2 Electrical Properties.....	10
2.2.3 Optical Properties	12
2.3 Nanowire Assembly	13
2.3.1 Dielectrophoresis (DEP) Theory	15
2.3.2 Dielectrophoresis of Nanowires	18
2.3.2 Previous Work on Nanowire Dielectrophoresis	26
2.4 Conclusion	30

TABLE OF CONTENTS (Continued)

	<u>Page</u>
3. EXPERIMENTAL TECHNIQUES	31
3.1 ZnO Nanowire Synthesis	31
3.1.1 Lindberg Furnace.....	32
3.1.2 Owen Furnace.....	34
3.1.3 Experimental Setup for Nanowire Growth.....	34
3.2 ZnO Nanowire Harvesting	36
3.3 Dielectrophoresis of ZnO Nanowires.....	37
3.3.1 Electrode Design	38
3.3.2 Fabrication of Substrate.....	39
3.3.3 Experimental Setup for Dielectrophoresis.....	40
3.3.4 DC Characterization	43
3.4 Conclusion.....	43
4. PARAMETERS AFFECTING NANOWIRE GROWTH	44
4.1 Design of Experiment.....	44
4.1.1 Effect of Growth Time.....	45
4.1.2 Effect of Gas Flow Rate.....	46

TABLE OF CONTENTS (Continued)

	<u>Page</u>
4.1.3 Effect of Deposition Temperature.....	47
4.2 Qualitative Density of Nanowires.....	48
4.3 Conclusion.....	51
5. NANOWIRE ALIGNMENT VIA DIELECTROPHORESIS.....	52
5.1 Effect of Bias.....	52
5.2 Effect of Frequency.....	54
5.3 Effect of Electrode Width.....	57
5.4 Effect of Setup.....	58
5.5 Removal of Excess Nanowires.....	60
5.6 Conclusion.....	62
6. ELECTRICAL AND PHOTORESPONSE MEASUREMENTS.....	63
6.1 Electrical Measurements.....	63
6.2 Photoresponse Measurements.....	71
6.3 Conclusion.....	73
7. CONCLUSIONS AND FUTURE WORK.....	74
7.1 Conclusions.....	74

TABLE OF CONTENTS (Continued)

	<u>Page</u>
7.2 Future Work	77
BIBLIOGRAPHY	79
APPENDICES	87
Appendix A Additional Images of Nanowire Removal	88
A.1 Align at 1 kHz, IPA Flush at 1 kHz-100 kHz and 1 kHz-200 kHz.....	88
A.2 Align at 1 kHz, IPA Flush at 1 kHz-100 kHz and 1 kHz-1 MHz.....	89

LIST OF FIGURES

<u>Figure</u>	<u>Page</u>
2.1 MOSFET structure incorporating nanowires between Source and Drain for the electrical characterization of nanowires	11
2.2 Photoresponse of a single ZnO nanowire from 254 nm and 366 nm UV modulation	12
2.3 A schematic showing the alignment of nanowires between two metal electrodes for positive DEP	18
2.4 $\text{Re}[K(\omega)]$ vs. Frequency for ZnO nanowires suspended in IPA.....	20
2.5 $\text{Re}[K(\omega)]$ vs. frequency at various medium conductivities ($\epsilon_n = 8.91\epsilon_0$, $\epsilon_m = 19.6\epsilon_0$, $\sigma_n = 2612 \text{ S/m}$).....	21
2.6 $\text{Re}[K(\omega)]$ vs. frequency at various medium permittivities ($\epsilon_n = 8.91\epsilon_0$, $\sigma_n = 2612 \text{ S/m}$, $\sigma_m = 1.79 \times 10^{-6} \text{ S/m}$).....	22
2.7 $\text{Re}[K(\omega)]$ vs. frequency at various nanowire conductivities ($\epsilon_n = 8.91\epsilon_0$, $\epsilon_m = 19.6\epsilon_0$, $\sigma_m = 1.79 \times 10^{-6} \text{ S/m}$)	23
2.8 $\text{Re}[K(\omega)]$ vs. frequency at various nanowire permittivities ($\epsilon_n = 19.6\epsilon_0$, $\sigma_n = 2612 \text{ S/m}$, $\sigma_m = 1.79 \times 10^{-6} \text{ S/m}$).....	24
2.9 (a) Forces besides F_{DEP} that act upon a nanowire in a microfluidic channel (b) Top view representation of electric field gradient (c) Side view representation of electric field gradient.....	25
2.10 Previous results of ZnO nanowire alignment through dielectrophoresis reported by (a) Lee <i>et al.</i> (b) Jiang <i>et al.</i>	30
3.1 A representation of the furnace setup in Kelley Nanolaboratory.....	32
3.2 Temperature profile of the (name) furnace when Zone 1 = 940, Zone 2 = 940 and Zone 3 = 670.....	33
3.3 A representation of the second furnace setup, whereby an additional O_2 inlet and a vacuum system are incorporated.....	34

LIST OF FIGURES (Continued)

<u>Figure</u>	<u>Page</u>
3.4 The experimental setup for nanowire growth.....	35
3.5 Sonication process for harvesting ZnO nanowires from a substrate.....	36
3.6 The layout of the substrate used for dielectrophoresis experiment.....	38
3.7 Experimental setup for Method 1 : (a) Narrow channel created with long rectangular silicon pieces (b) Tilted substrate for nanowire solution flow.....	41
3.8 Experimental setup for Method 2 – alignment of nanowires through dielectrophoresis force and capillary force	42
4.1 Qualitative Growth Density of ZnO nanowires vs. (a) Growth Time – flow rate = 150 sccm, deposition temperature = 850°C (b)Flow Rate – growth time = 60 minutes, deposition temperature = 850°C and (c) Deposition Temperature – growth time = 60 minutes, flow rate = 150 sccm, on ZnO and Al ₂ O ₃ /ZnO seed layers.....	49
4.2 SEM image of ZnO nanowires grown on Al ₂ O ₃ /ZnO seed layer. (Growth time = 60 minutes, flow rate = 150 sccm, deposition temperature = 850°C).....	50
5.1 Dark field optical microscope images showing the effect of bias on Nanowire deposition: (a) -5 V to 5 V (b) 0 V- 10 V (Frequency = 10 kHz, nanowire solution volume = 125 μL, gap = 5 μm)	53
5.2 Dark field images of nanowires aligned at 10 V _{pp} and varying frequencies: (a) 10 Hz (b) 100 Hz (c) 1 kHz (d) 10 kHz (e) 100 kHz (f) 200 kHz (g) 1 MHz.....	55
5.3 Number of wires attracted and average angle of alignment at various frequencies (V _{pp} = 10 V)	57
5.4 Comparison of nanowire distribution between (a) Setup 1 and (b) Setup 2, on a 5 μm gap.....	59

LIST OF FIGURES (Continued)

<u>Figure</u>	<u>Page</u>
5.5 Alignment of nanowires at 10Vpp, 10kHz (a) without removal of overlapping nanowires, and (b) with removal of overlapping wires through frequency tuning (10kHz to 100kHz) and IPA flush, on the same 5 μ m gap.....	61
5.6 Alignment of nanowires at 10Vpp, 10kHz (a) without removal of overlapping nanowires, and (b) with removal of overlapping wires through frequency tuning (10kHz to 1 MHz) and IPA flush, on the same 5 μ m gap.....	61
6.1 Representation of dielectrophoretically-aligned nanowires (a) on bottom metal contacts and (b) with additional top metal contacts.....	64
6.2 A comparison of number of aligned/bridging nanowires (a) before sonication (b) after 10 seconds sonication on a 0.2 mm long, 5 μ m wide gap.....	66
6.3 A comparison of current vs. normalized E-field behavior of dielectrophoretically aligned ZnO nanowires with only bottom contact, and with additional top contact.(inset)-data in log scale.....	66
6.4 Possible current leakage paths in a MOSFET device.....	67
6.5 I-V measurements showing (a) Leakage current vs. drain voltage (b) Drain current vs. drain voltage, with gate control ($V_g = -10V, 0V, 10V$).....	68
6.6 Photoresponse obtained by continually switching the UV light on and off at an applied bias of 3 V.....	70

LIST OF TABLES

<u>Table</u>	<u>Page</u>
3.1 Measured temperatures at 35 cm and 45 cm from the left edge of the Lindberg furnace at different temperature settings for Zones 1,2, and 3.....	33
4.1 The design matrix and results for the study of growth time effect on nanowire growth. Constant parameters employed are: flow rate = 150 sccm, deposition temperature = 850°C).....	45
4.2 The design matrix and results of flow rate effect on nanowire growth. Constant parameters employed are: growth time = 60 min, deposition temperature = 850 °C.....	47
4.3 The design matrix and results of deposition temperature effect on nanowire growth. Constant parameters employed are: growth time = 60 min, flow rate = 150 sccm.....	48

INTEGRATION OF VAPOR-SOLID GROWN ZnO NANOWIRES THROUGH DIELECTROPHORESIS

1. INTRODUCTION

Nanostructures are described as structures that are 1 to 100 nm in at least one dimension [1]. They can be further classified as 0-D, 1-D and 2-D nanostructures, in which examples of each type include nanoparticles, nanowires and thin films respectively [2]. The research on nanowires is gaining momentum due to their potential in various applications namely electronics, biomedical science, defense, etc. [3]. As an example, Zinc Oxide (ZnO) nanowires are employed as a chemical-sensing element in microelectronic devices [4]. An advantage in utilizing materials such as metal oxides in their nanoscale form is that the increased surface area-to-volume ratio compared to their microscale counterpart allows for improved sensitivity since most sensing reactions occur on the surface of a material [2,5].

To date, much work has been conducted on nanostructures of materials including carbon (C), silicon (Si), germanium/silicon (Ge/Si), selenium (Se), tellurium (Te), gallium nitride (GaN), gallium arsenide (GaAs), palladium (Pd) and molybdenum (M) [1,3,6-9]. This thesis will focus solely on zinc oxide (ZnO) nanowires.

ZnO, which belongs to the wurtzite crystal structure, is composed of zinc atoms tetrahedrally arranged with four oxygen atoms [10]. With properties such as a wide bandgap of $\sim 3.37\text{eV}$ at room temperature and large exciton binding energy (60 meV) that renders efficient exciton emission compared to other semiconductors, ZnO has been touted as an excellent semiconductor, in particular for UV lasing applications

[11]. Apart from that, ZnO has a high piezoelectric constant, which is advantageous in mechanical devices such as actuators and transducers [12,13].

One of the many challenges in nanomaterials research is the assembly of these tiny structures. In the application of nanowires for modern electronic devices, a single nanowire or an array of nanowires is connected between two electrodes in order to investigate its electrical properties. In addition, a back-gate or top-gate electrode is employed to provide a means of control over channel conduction in a metal-oxide semiconductor field effect transistor (MOSFET) structure [11,14,15]. The direct and indirect approaches are two of the most common methods used to integrate nanowires between electrodes. In the direct approach, nanowires, or rather, nanobridges are grown from photolithography-patterned electrodes during chemical vapor deposition process [16,17,18]. In the indirect approach, nanowires are grown on a substrate, and later harvested, generally through ultrasonication [19] so that the fluid-suspended nanowires can be transferred to a test device [15]. Methods of transfer include random dispersion of nanowire solution, microchannel assisted flow, as well as electrical manipulation of nanowires in solution, also known as dielectrophoresis (DEP).

Although the research on dielectrophoresis of nanowires has gained momentum in the last few years [20-47, 48, 49], none have reported how excess or nonbridging nanowires can be removed through frequency tuning. Improving the assembly of nanowires is crucial if the nanowires are to be incorporated in a device. Long wires, or rather, wires that are not perpendicularly bridged within the electrodes cause longer conducting paths, and hence slower devices. On the other hand, short

wires that do not bridge are simply leaking or wasting current. Therefore, the objective of this thesis is to study the alignment behavior of nanowires using dielectrophoresis, and to investigate how excess nanowires can be removed by tuning the frequency of the electric field applied. In addition, the electrical and UV sensing properties of the formed devices will be tested.

2. LITERATURE REVIEW AND TECHNICAL BACKGROUND

This chapter reviews some of the extensive research that has been conducted in the fabrication and characterization of nanowires. A review on the theory and concept of dielectrophoresis will be presented as well to provide the reader a better understanding on how nanowires can be manipulated or assembled from fluidic suspension.

2.1 Nanowire Synthesis Methods

To date, many synthesis methods have been reported for the fabrication of nanowires. Depending on factors such as the desired final application or processing limitations, the bottom-up approach is generally preferred over top-down since the latter generates more impurities and defects from processing procedures, in particular etching [2]. Also, after 40 years of scaling to smaller dimensions, the top-down approach is quickly reaching its physical and economic limits, thereby making the bottom-up approach more favorable [5].

Before the details of synthesis methods are presented, it would be beneficial to comprehend the theory behind crystal growth. According to Cao [2], the driving force for spontaneous growth is the decrease in Gibbs free energy, and a typical heterogeneous crystal growth process can be outlined as follows:

1. Diffusion of growth species in their bulk form, either in vapor or liquid phase,

onto the desired growth surface

2. Adsorption and desorption of growth species onto and from the growing surface
3. Surface diffusion of adsorbed growth species, whereby the latter may either be incorporated into a growth site or escape from the surface
4. Irreversible incorporation of growth species into crystal structure when sufficient supersaturation is achieved
5. Desorption and diffusion of by-products from the growth surface

Since the bottom-up growth methods result in higher quality nanowires and thus will be used for this research, the sections to follow will only delve into details of nanowires grown via bottom-up methods.

2.1.1 Vapor-Liquid-Solid

The Vapor-Liquid-Solid (VLS) method requires the use of a metal catalyst, typically gold (Au) [13,50,51], although silver (Ag) catalyst has been reported as well [52] for the growth of ZnO nanowires.

The catalyst of choice is usually deposited as a thin film (~10-20nm) on a Si-substrate. When the coated substrate is placed in the furnace at a temperature near the catalyst/Si eutectic point, liquid droplets of the catalyst start to form. At the same time, the source material that is being evaporated is transported to the substrate region and absorbs the surface of the catalyst/Si droplet. When the liquid catalyst is

supersaturated with source vapor, nucleation occurs, causing the growth of nanowires.

Although the VLS method is preferred for ease of selective growth [2], its most significant drawback is that when a metal catalyst is introduced, the nanowires grown may be contaminated, thus altering their properties [1,53].

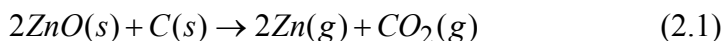
2.1.2 Vapor-Solid

As the name suggests, the vapor-solid (VS) synthesis method entails the evaporation of a source material at its melting temperature, followed by the transport of the source vapor via an inert gas flow, such that the gas species can be adsorbed onto a growth surface at a lower temperature region. Subsequently, nanowires will grow spontaneously once supersaturation of the growth species is achieved [2].

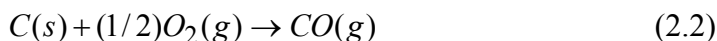
The most straightforward method in growing ZnO nanowires would be through evaporating Zn or ZnO powder near its melting temperature and condensing the gas species at a lower temperature so that crystal growth process as outlined earlier would take place [54-56].

Besides the direct thermal evaporation approach, one group have reported successful findings through the carbothermal reduction method [57]. In this process, high purity ZnO powder is mixed with graphite and placed in a furnace at a high temperature of $\sim 900^{\circ}\text{C}$ - 1100°C . According to Yao *et al.* in 2002 [57], when a

mixture of ZnO powder and carbon is placed in a high temperature furnace, the reaction that takes place can be represented by the following equation:



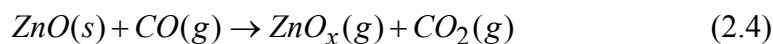
In this reaction, carbon reduces ZnO into Zn - which plays an important role in the nucleation of ZnO nanowires. Regardless of whether the ends of the tube furnace is opened to atmosphere or sealed with a controlled amount of oxygen introduced, the following reaction takes into effect:



Therefore, carbon not only reacts with ZnO but also with oxygen, to produce carbon oxide. Hence, the combined reaction can be modeled as follows:



Yao *et al.* [57] also further postulated that with the presence of oxygen, Zn suboxides are produced, hence contributing to the nucleation of ZnO nanowires as well. The following equation describes this reaction,



where the subscript x is <1 .

Also, since Zn or Zn suboxides have lower melting temperature (~ 419 °C) compared to ZnO (~ 1975 °C), carbothermal reaction requires a lower operating temperature in contrast to direct evaporation of ZnO.

Another synthesis route worth mentioning is the metal organic chemical vapor deposition process (MOCVD). In 2008, Baxter and Aydil [58] reported the synthesis of ZnO nanowires using hydrated zinc acetylacetonate ($\text{Zn}(\text{acac})_2$) as the source material, which only required 75°C to evaporate. Part of their findings included the morphology of the growth process, which saw the transformation from a polycrystalline film to nanowires to secondary nanowires. The change in morphology also corresponded to the change in the precursor material, where the initial hydrated $\text{Zn}(\text{acac})_2$ converted into anhydrous $\text{Zn}(\text{acac})_2$, followed by ZnO [58]. The group also stated that this method is advantageous in that it 1) demands lower temperature compared to thermal evaporation; 2) provides higher purity material than solution method; and 3) does not require carbon as the precursor.

2.1.3 Hydrothermal

In hydrothermal growth, the growth species is dissolved into a solution, where it diffuses and deposits onto a growth surface, resulting in nucleation and growth of nanowires [2]. Kar *et al.* [59] in 2009 reported hydrothermal growth of ZnO nanowires at 75°C using an equimolar (0.005 M) aqueous solution of zinc nitrate ($\text{Zn}(\text{NO}_3)_2 \cdot 6\text{H}_2\text{O}$) and hexamethyltetramine (HMT, $\text{C}_6\text{H}_{12}\text{N}_4$). The process took 8 hours to complete [31].

In another study, Wen *et al.* [60] conducted a hydrothermal growth with similar source material and solution as Kar *et al.* [59], but with the addition of a

surfactant, cetyltrimethylammoniumbromide (CTAB) to the solution, which acts as controlling agent to the final shape of the nanostructures. Also, the solution was stirred for 2 hours with the growth substrate immersed, and subsequently transferred to a sealed autoclave that was heated to 80°C [60].

The major advantage in utilizing the hydrothermal method is that high-temperatures are not necessary, hence lowering the cost of fabrication [53]. However, compared to the VS or VLS method, the hydrothermal approach requires longer synthesis duration.

2.2 Nanowire Characterization

The most common properties that have been explored of nanowires are their physical, electrical and optical properties. The following sub-sections will detail the methods in nanowire characterization.

2.2.1 Physical Properties

Nanowires are commonly characterized by their length, diameter, uniformity on a substrate, growth density and alignment [57,61]. Scanning electron microscopy (SEM) is one of the most widely used techniques in obtaining images of nanostructures for characterization. In SEM operation, a source of electrons accelerated up to 50 KeV is focused by a beam and rastered over the sample by deflection coils. Electrons and photons would then emit from the sample as a result of

a number of interactions from source electrons striking and penetrating the sample. The emitted electrons are collected through a cathode ray tube (CRT), which in turn produces SEM images [2].

Besides SEM, transmission electron microscopy (TEM) is also often used in the characterization of nanowires. The mechanism of TEM is similar to SEM, but with a higher acceleration of source electrons (100 KeV-1MeV) and a higher magnification ($50 - 10^6$), TEM allows for image and diffraction information from a single sample. Crystalline defects such as dislocation and stacking fault can be imaged through TEM, as can the crystallinity of nanostructures, e.g. single crystalline or amorphous [57].

2.2.2 Electrical Properties

Since nanowires are proposed in the application of modern electronic devices, their electrical properties are often studied. The most common way is by incorporating nanowires between two electrodes, which mimic the Source (S) and Drain (D) of a MOSFET. The nanowires can either be grown directly on pre-patterned electrodes, or grown separately followed by the dispersion of sonicated nanowires in solution onto the region between Source and Drain. Figure 2.1 shows the configuration of a MOSFET structure with nanowires incorporated between Source and Drain.

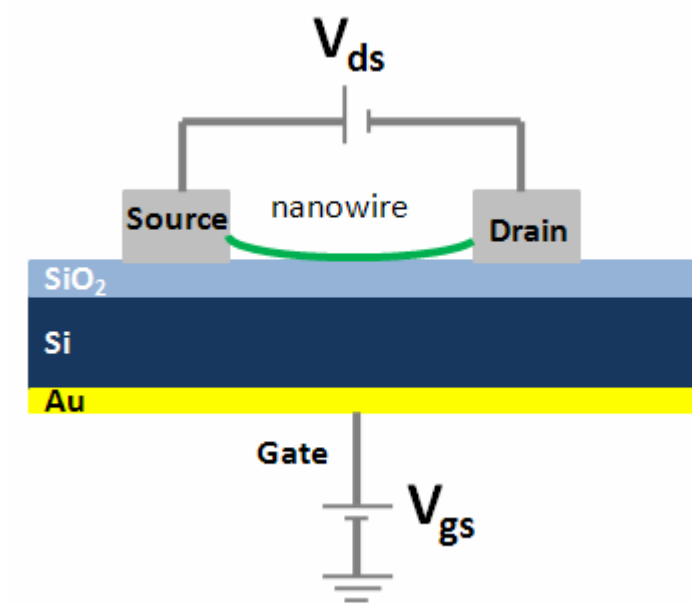


Figure 2.1 MOSFET structure incorporating nanowires between Source and Drain for the electrical characterization of nanowires.

Often times, the drain current, I_d versus Drain-Source Voltage, V_{ds} is explored, along with drain current, I_d versus Gate Voltage, V_g with varying V_{ds} . The I_d vs. V_{ds} curve will portray the contact behavior between the nanowire and the contact electrodes, i.e. Ohmic or Schottky, while other parameters such as carrier mobility, transconductance, ‘on’ current, and drain current at various V_{ds} and V_g can be obtained from the I_d vs. V_g curve [14,21].

2.2.3 Optical Properties

The optical properties of nanowires are of interest since they are highly sensitive to the chemical environment due to their large surface area. For example, a carbon monoxide (CO) molecule can increase the number of electrons on the surface of a ZnO nanowire, thus rendering it more photoconductive [4].

Figure 2.2 shows the photoresponse of the single ZnO nanowire under pulsed illumination from a 254 nm and a 366 nm wavelength Hg lamp. The lower photocurrent from the 254 nm illumination was attributed to more efficient absorption near the nanowires surface, and the fact that the peak photocurrents were fairly constant was due to the discharge of traps during measurement [52].

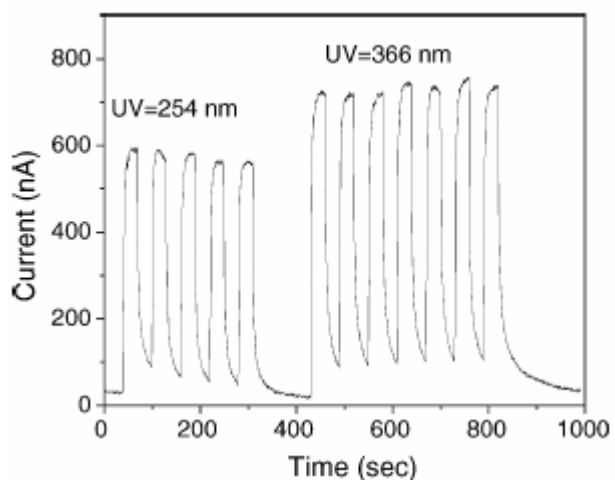


Figure 2.2 Photoresponse of a single ZnO nanowire from 254 nm and 366 nm UV modulation (Figure taken from [52]).

2.3 Nanowire Assembly

The assembly of nanowires in between electrodes is essential for making useful devices. Several different methods of assembly that have been investigated include physical transfer, direct growth of nanobridges, pick and place, and dielectrophoresis (DEP).

In the physical transfer method, nanowires that are grown on a substrate are rubbed against another substrate in order to separate the nanowires from the growth substrate. This method also produces random placement of nanowires and will not be a good choice for creating devices since uniformity is not controlled.

In the direct growth of nanobridges method, substrates with lithographically pre-defined electrodes are used in the nanowire growth chamber so that wires can grow across the electrodes. The drawback to this method is that the number of wires bridging the electrodes is difficult to control and the substrate is exposed to high temperature from nanowire growth.

In the pick and place method, nanowires are grown on a substrate, harvested in solution and dispersed randomly on another substrate. Electrodes are then deposited on the ends of the dispersed nanowires either individually or via lithography to create devices. Since the nanowires are randomly placed, this poses a challenge in making uniform devices.

Using DEP is a potential solution since nanowires are manipulated through voltage and frequency control to specified regions of electrodes that have been pre-

defined and fabricated. DEP is an emerging technique for the alignment of inorganic nanowires. Unlike assembly via direct nanowire growth which requires a much higher temperature, DEP can be performed at room temperature. Therefore, the device substrate used during nanowire assembly is separated from high temperature growth process. DEP has the possibility of providing better control over the number of wires aligned, and hence more uniform device performance. In addition, the use of DEP for nanowire assembly is compatible with current IC fabrication processes where the metal contacts in a typical MOSFET structure can be utilized as the alignment electrodes. Because growth is separated from assembly, DEP is a cleaner option as opposed to growing nanobridges in a CVD chamber, and hence reduces the risk of contamination if used in a manufacturing environment. A drawback to DEP is that since the nanowires are only lying on the electrodes, a top contact is often necessary to ensure good Ohmic contact. Also, since DEP requires the sonication of nanowires, various nanowire lengths may be produced, which could cause low yielding of bridging wires. However, the potential advantages of DEP make it an interesting topic for research.

In the next subsections, the theory of DEP will be discussed, as well as the assembly of nanowires using DEP.

2.3.1 Dielectrophoresis (DEP) Theory

Dielectrophoresis was traditionally used in the ceramics industry [22], but because of the emerging interest in nanotechnology, it has found its way in the assembly of various nanostructures, be it for biotechnology [48] or microelectronics applications [47]. In biotechnology, dielectrophoresis is commonly used to separate cells, where more spherical structures are dealt with rather than elongated structures such as nanowires in microelectronics. The dielectrophoresis phenomenon was first discovered by Pohl [62] in the 1950's, and was defined as the motion of uncharged, polarizable particles due to induced dipole moments in the nanoparticles and the suspending medium due to the presence of a nonuniform electric field [62]. Following Pohl [62], the general expression for dielectrophoresis force is as follows

$$\vec{F}_{DEP}(t) = [\vec{p}(t) \bullet \nabla] \vec{E}(t) \quad (2.5)$$

where $\vec{p}(t)$ is the induced dipole moment vector, and $\vec{E}(t)$ the time-varying applied electric field. For an isotropic, linear and homogeneously polarizable particle, the dipole moment vector is dependent upon the electric field, as shown below:

$$\vec{p}(t) = \alpha V \vec{E}(t) \quad (2.6)$$

where α is the polarizability tensor for the particle, and V is the total volume of the particle. Substituting Equation 2.6 into Equation 2.5 yields the following:

$$\vec{F}_{DEP} = \frac{1}{2} \alpha V \nabla |E^2| \quad (2.7)$$

For a cylindrical particle such as a nanowire, α is defined as the following [37]:

$$\alpha = \varepsilon_m \operatorname{Re}[K(\omega)] \quad (2.8)$$

where ε_m is the real permittivity of the medium and $\operatorname{Re}[K(\omega)]$ is the real part of the Clausius-Mossotti factor. The dielectrophoresis force equation can be further expanded into the following:

$$\vec{F}_{DEP} = \frac{1}{2} V \varepsilon_m \operatorname{Re}[K(\omega)] \nabla(\vec{E}_{rms}^2) \quad (2.9)$$

where V is the volume of the particle, and E_{rms} is the root mean square value of the electric field.

One should also note the difference between electrophoresis and dielectrophoresis. In electrophoresis, a charged particle is pulled along the electric field lines toward the electrode with opposite charge. The reversal of the field would reverse the direction of travel of the charged particle. Electrophoresis is observable on particles of any size which can include atomic ions, molecular ions, charged colloidal particles, or charged macroscopic bodies. Also, the free charge on a particle plays a more important role than the volume in electrophoresis [62].

In dielectrophoresis, a neutral particle in a nonuniform electric field experiences polarization and hence becomes positively charged on the side closer to the negative electrode and vice versa. Although the number of positive and negative charges on each side of the neutral particle is equal, separation creates a field between the two regions, thus resulting in a net force. The net force causes the particle to move toward the region of stronger field.

According to Pohl [62], the magnitude and direction of the induced dipole strongly depend on the frequency and magnitude of the applied electric field. When the applied field is non-uniform, a liquid-suspended particle experiences Coulombic force of different magnitudes on either side. A net force is exerted in the direction where the electric field is greatest, thus causing the particle to move along the direction that experiences the highest electric field gradient. Also, dielectrophoresis is observed for both DC and AC fields [20,24]. An important fact is that in dielectrophoresis, the motion of the polarized particle is independent of the direction of the electric field polarity. The volume of a particle plays an important role in dielectrophoresis and therefore it is more observable on coarse particles.

Dielectrophoresis can be further defined as positive DEP or negative DEP. When the complex dielectric permittivity of the particle is greater than that of its suspending liquid medium, the polarized particle will be pulled towards the high electric field region (positive DEP), and the opposite is true for negative DEP [25-28]. Figure 2.3 shows a schematic for positive DEP, where the majority of nanowires are attracted in the region of highest electric field, i.e. between the two electrodes.

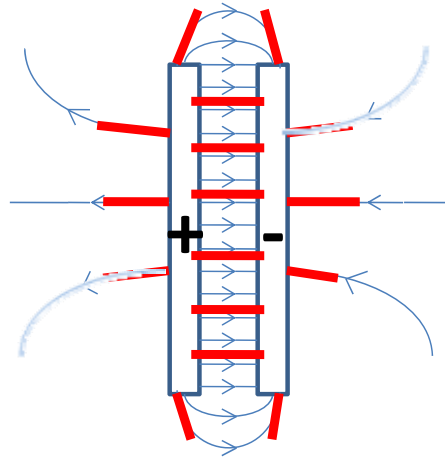


Figure 2.3 A schematic showing the alignment of nanowires between two metal electrodes for positive DEP.

2.3.2 Dielectrophoresis of Nanowires

The dielectrophoresis force, \vec{F}_{DEP} i.e. the most basic parameter in understanding dielectrophoresis for nanowire assembly. Substituting the volume of a cylindrical particle into equation 2.9, the following expression is obtained:

$$\vec{F}_{DEP} = \frac{\pi r^2 l}{2} \epsilon_m \text{Re}[K(\omega)] \nabla (\vec{E}_{rms}^2) \quad (2.10)$$

where r is the radius of the nanowires, l is the length of the nanowires, ϵ_m is the dielectric constant of the liquid medium, $\text{Re}[K(\omega)]$ is the real part of the Clausius-Mossotti factor, and \vec{E}_{rms} is the root mean square value of the electric field. The equation for $\text{Re}[K(\omega)]$ can be expanded into the following:

$$\text{Re}[K(\omega)] = \text{Re}\left[\frac{\varepsilon_n^* - \varepsilon_m^*}{\varepsilon_m^*}\right], \quad (2.11)$$

$$\varepsilon_n^* = \varepsilon_n - i\frac{\sigma_n}{\omega}, \quad \varepsilon_m^* = \varepsilon_m - i\frac{\sigma_m}{\omega} \quad (2.12)$$

where ε_n^* is the complex permittivity of the nanowire, ε_m^* is the complex permittivity of the liquid medium, ε_n (ε_m) is the real permittivity of the nanowire(liquid), and can be written as $\varepsilon = \varepsilon_p \times \varepsilon_o$, where ε_p and ε_o are the relative and free-space permittivity, respectively. σ_n (σ_m) is the conductivity of the nanowire(liquid), and ω is the frequency. It must be noted that the complex permittivity varies as a function of frequency [21,26].

Clearly, equations 2.11 and 2.12 show that the dielectrophoresis force is governed by the gradient and the frequency of the electric field applied, respectively. However, frequency plays a critical role since permittivity is highly dependent upon the frequency [62]. Depending on the nanowire material and the suspending liquid medium, the optimized frequency for maximum F_{DEP} may differ, and therefore needs to be scrutinized. Finding the maximum F_{DEP} is crucial for high yielding nanowire bridges between the alignment electrodes. Understanding the frequency response of F_{DEP} is important for controlled flushing of excess or overlapping nanowires.

According to several studies [14,21,28,48], a distinct cutoff frequency exists from the maximum to the minimum value of $\text{Re}[K(\omega)]$. Specifically for the case of ZnO nanowires suspended in IPA - which was the condition for this research, both Kumar *et al.* [48] and Lee *et al.* [21] reported in 2009 that the $\text{Re}[K(\omega)]$ is maximum

from 10 Hz but begins to roll off at 10 kHz, and reaches its minimum from 1 MHz and beyond. Figure 2.4 shows the characteristic curve of the $\text{Re}[K(\omega)]$ vs. frequency for ZnO nanowires suspended in IPA reported by Kumar *et al* [48].

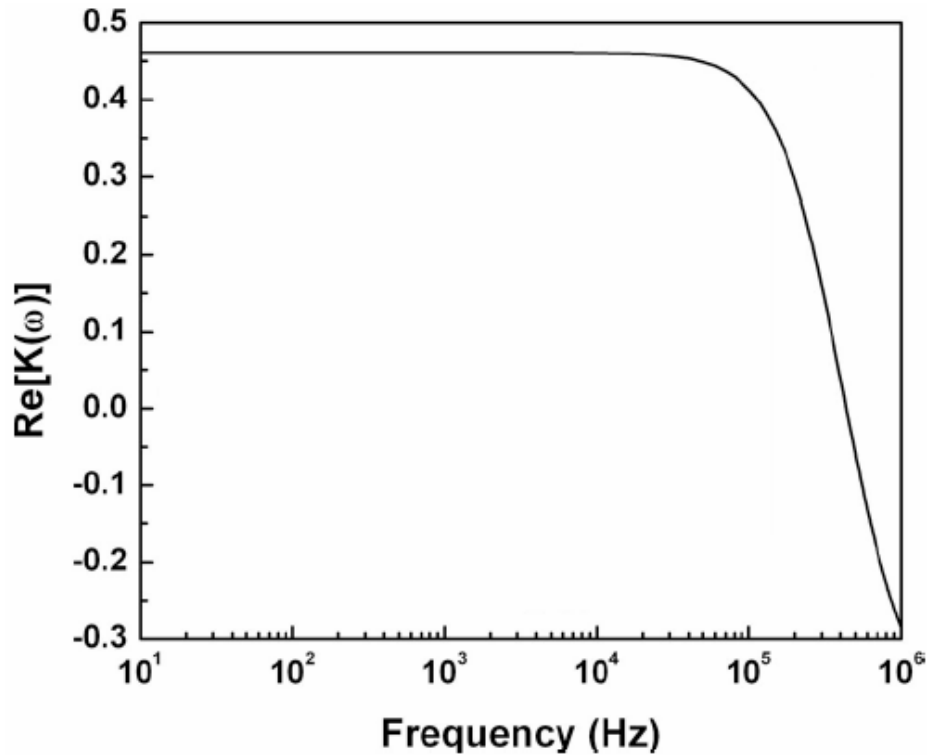


Figure 2.4 $\text{Re}[K(\omega)]$ vs. frequency for ZnO nanowires suspended in IPA [48].

To understand how the conductivity and permittivity of the nanowire and the suspending liquid medium affect the $\text{Re}[K(\omega)]$ - which is proportional to the dielectrophoresis force, calculations have been carried out [63], whereby only one parameter is varied at a time. For a cylindrical particle, the frequency response for the real part of Clausius-Mossotti factor, $\text{Re}[K(\omega)]$ can be modeled as follows [23]:

$$\text{Re}[K(\omega)] = \frac{\omega^2 \varepsilon_m (\varepsilon_n - \varepsilon_m) - \sigma_m (\sigma_m - \sigma_n)}{\omega^2 \varepsilon_m^2 + \sigma_m^2} \quad (2.13)$$

where ω is the frequency, ε_m is the permittivity of the liquid medium, ε_n is the permittivity of the nanowire, σ_m is the conductivity of the liquid medium, and σ_n is the conductivity of the nanowire.

Figure 2.5 shows that with fixed ε_n , ε_m , and σ_n , the drop in F_{DEP} occurs at a higher frequency as the conductivity of the medium increases.

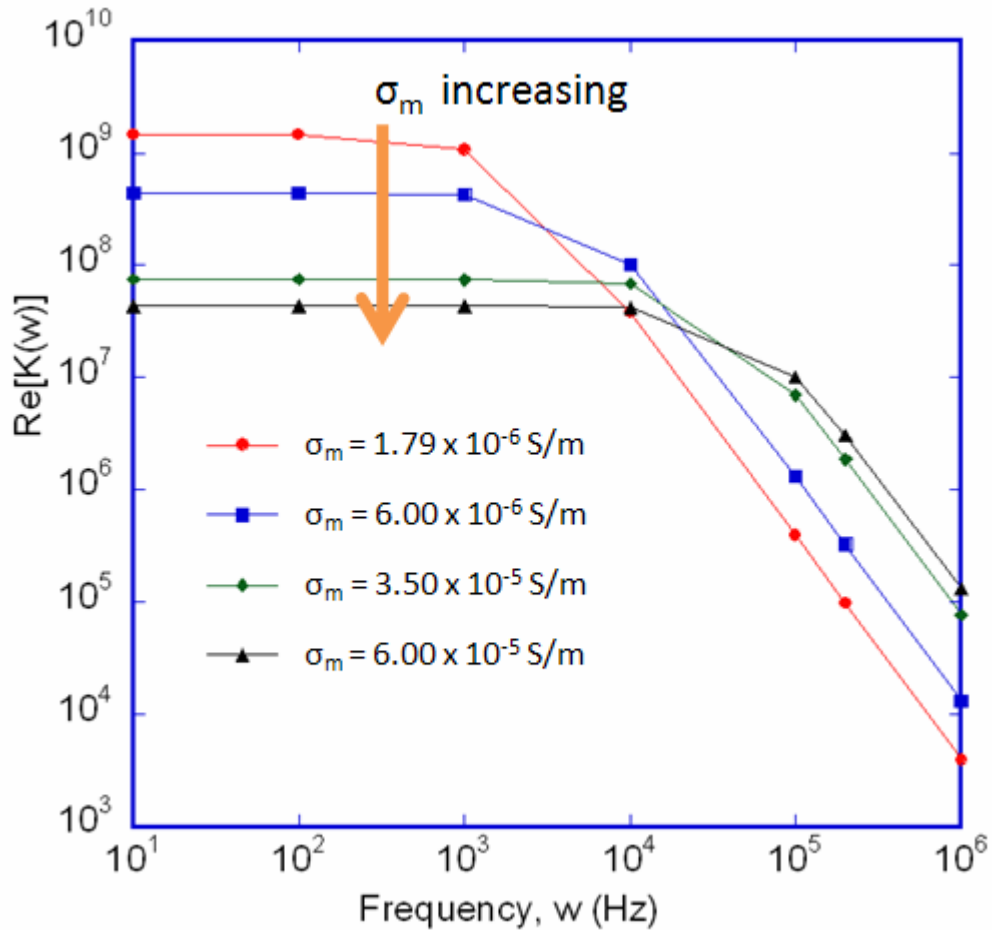


Figure 2.5 $\text{Re}[K(\omega)]$ vs. frequency at various medium conductivities. ($\varepsilon_n = 8.91\varepsilon_0$, $\varepsilon_m = 19.6\varepsilon_0$, $\sigma_n = 2612$ S/m) [63].

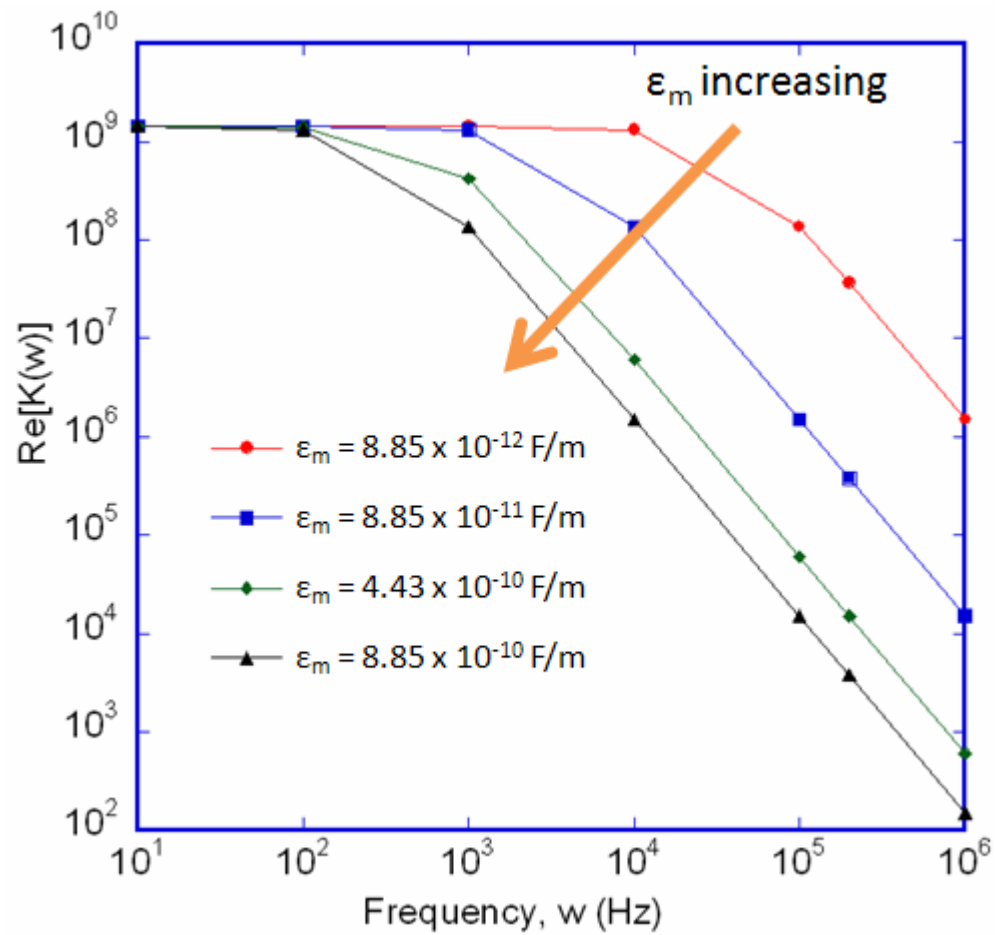


Figure 2.6 $\text{Re}[K(\omega)]$ vs. frequency at various medium permittivities. ($\epsilon_n = 8.91\epsilon_0$, $\sigma_n = 2612 \text{ S/m}$, $\sigma_m = 1.79 \times 10^{-6} \text{ S/m}$) [63].

However, when the permittivity of the medium is varied and ϵ_n , σ_n , and σ_m are fixed, the drop in F_{DEP} occurs at a higher frequency as the permittivity of the medium decreases. Figure 2.6 shows the results.

On the other hand, calculations carried out varying the conductivity and permittivity of nanowires show that these two parameters do not play a role in the

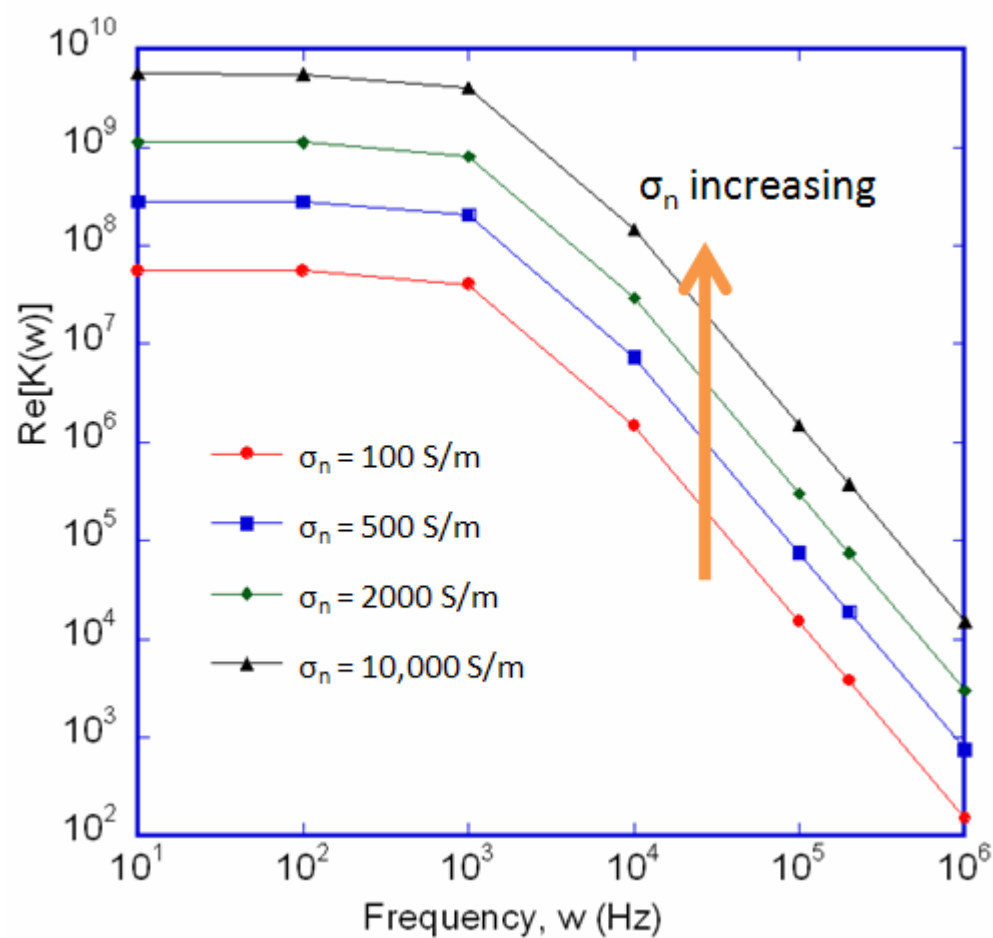


Figure 2.7 $\text{Re}[K(\omega)]$ vs. frequency at various nanowire conductivities. ($\epsilon_n = 8.91\epsilon_0$, $\epsilon_m = 19.6\epsilon_0$, $\sigma_m = 1.79 \times 10^{-6}$ S/m)[63].

frequency dependent behavior as seen from Figures 2.7 and 2.8. Only the magnitude of the $\text{Re}[K(\omega)]$ is affected when the conductivity of the nanowires is varied. Figure 2.7 shows this result, where the higher the conductivity of the nanowires, the higher the $\text{Re}[K(\omega)]$.

When the permittivity of the nanowires is varied, neither the change in the magnitude of $\text{Re}[K(\omega)]$ nor frequency behavior is observed. Figure 2.8 depicts this finding where the frequency response for all nanowire permittivities is the same.

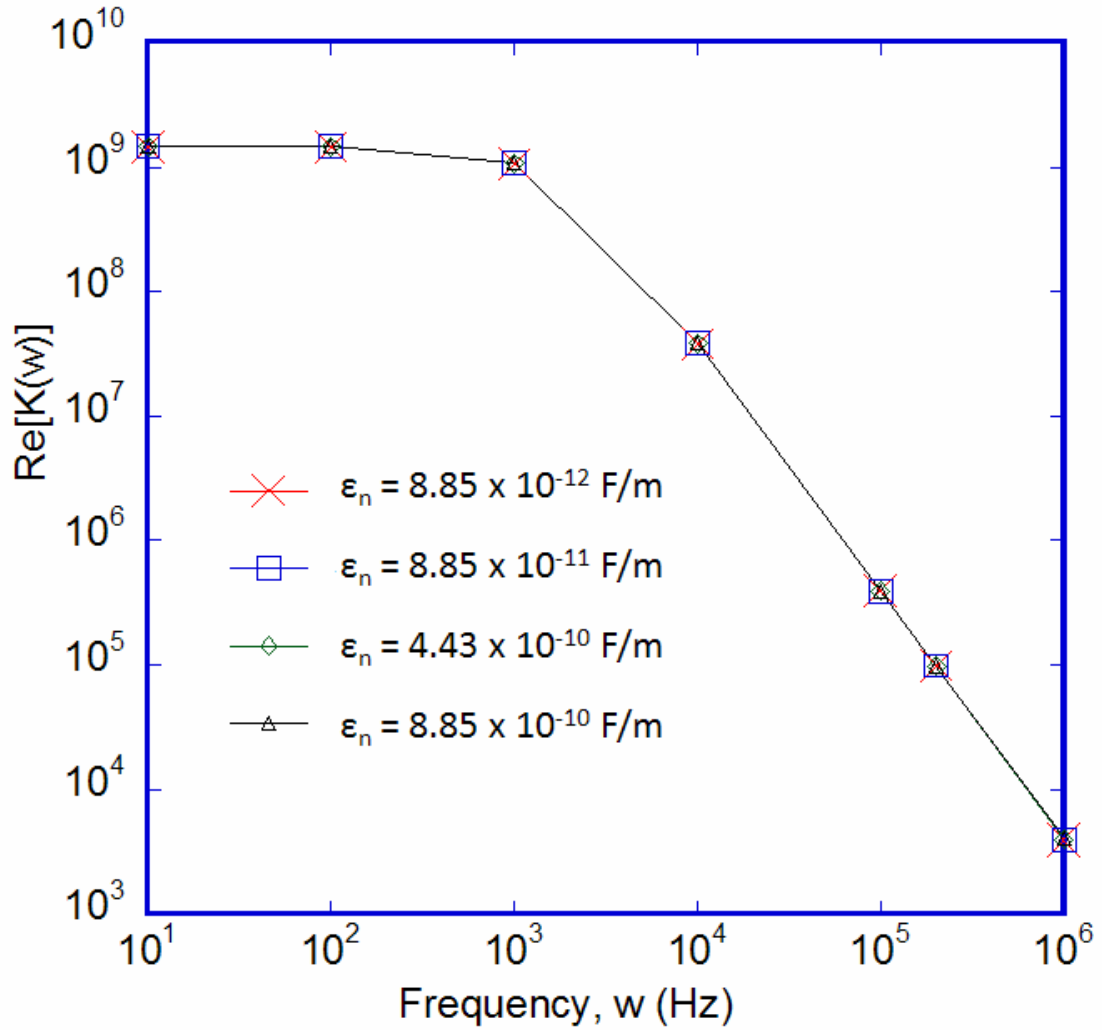


Figure 2.8 $\text{Re}[K(\omega)]$ vs. frequency at various nanowire permittivities. ($\epsilon_m = 19.6\epsilon_0$, $\sigma_n = 2612$ S/m, $\sigma_m = 1.79 \times 10^{-6}$ S/m) [63].

From Figures 2.5 – 2.8, it is seen that the conductivity and permittivity of the liquid medium play a more important role than the conductivity or permittivity of the nanowire in determining the optimized frequency for dielectrophoresis force.

Besides dielectrophoresis force, a number of other forces need to be considered for optimization. According to Lee *et al.* [21], other forces that act upon nanowires in a

microfluidic channel include drag force (F_{drag}), buoyancy force (F_{buoy}), and gravitational force (F_{grav}). Figure 2.9 (a) depicts these forces.

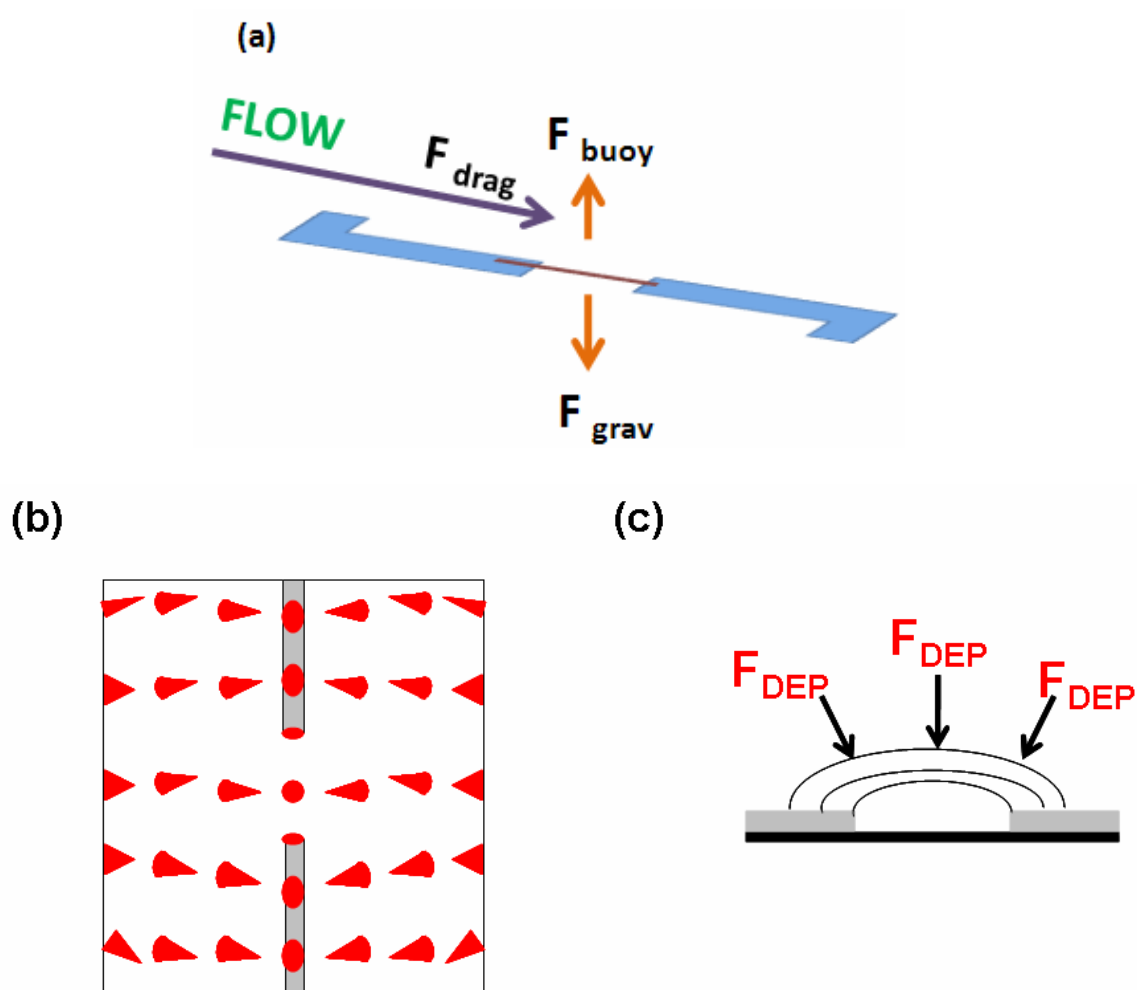


Figure 2.9 (a) Forces in addition to F_{DEP} that act upon a nanowire in a microfluidic channel (adapted from [21] and [30]) (b) Top view representation of electric field gradient (adapted from [30]) (c) Side view representation of electric field gradient (adapted from [30])

A three-dimensional finite element analysis performed by Raychaudhuri *et al.* [30] revealed that a nanowire will be aligned between two electrodes when it moves along the gradient of the electric field. Figure 2.9 (b) and (c) show the top view and side view representations of the electric field gradient. Since from Equation 2.9 F_{DEP} is proportional to the gradient of the electric field, this means that the direction of F_{DEP} is similar to the direction of the electric field gradient, as shown in Figure 2.9 (c).

It is important that the dielectrophoresis force be larger than the drag force. Otherwise, if drag force dominates, the flow of nanowires would only bypass the electrode gap and not be trapped as hoped. To avoid this situation, either (i) maximize F_{DEP} by using the optimized ϵ_m or σ_m , or (ii) reduce the flow rate of the nanowires to minimize drag force.

Lee *et al.* [21] also pointed out that the gravitational force, F_{grav} , will be larger than the buoyancy force, (F_{buoy}), if the density of the nanowire is larger than that of the liquid medium. In this case, the nanowires will eventually settle on the substrate surface regardless of F_{DEP} and F_{drag} .

2.3.3 Previous Work on Nanowire Dielectrophoresis

One of the earliest works published on dielectrophoresis of nanostructures was one that pertained to single-wall carbon nanotubes (SWCNTs) in 2001 [29]. The conclusion drawn from this study was that at high frequencies, namely at 5 MHz, the CNTs aligned were highly oriented, and fewer larger particles were present. Since

then, the concept of dielectrophoresis for nanowire or nanoparticle assembly has been employed for a variety of materials, including InAs [30], Pd [31], GaN [26, 32-35], CdSe [36], Au [37], NiSi [38], SiC/CNT [39], ZnO [21] and Au-Ag-Au [40]. Although the most common use of dielectrophoresis is to align wires between two electrodes, some groups have found additional interesting uses for DEP, such as fabricating hybrid wires (e.g. NiSi and SiC/CNT) and trapping Ag nanoparticles in between two Au nanowires that have been aligned dielectrophoretically [40].

The most reported work on dielectrophoresis of nanowires so far has been on ZnO [14,43,45,60-63,71] perhaps due to its widespread interest. Another metal oxide that has utilized dielectrophoresis for nanowire assembly is SnO₂ [41]. The two most common liquid medium used with ZnO reported were ethanol and IPA. The general observation is that a higher frequency is required for optimization when using ethanol, e.g. 100 kHz [42], 1 MHz [43, 44], and 10 MHz [45]. Conversely, a lower frequency, i.e. 10 kHz [14,21] has been shown to give optimized alignment conditions when IPA is used as the suspension medium.

Raychaudhuri *et al.* [30] conducted a study on the frequency dependence of dielectrophoresis force using InAs nanowires dispersed in deionized (DI) water. They found that maximum force was observed from 1 Hz to 10 kHz and a steep drop occurred from 10 kHz. A similar behavior has also been reported by Motayed *et al.* in 2006 [35], but using GaN suspended in IPA. In another study involving GaN suspended in IPA, Lee *et al.* [26] presented data that showed more wires attracted at 10 kHz than at 20 MHz.

Since according to Pohl [62], dielectrophoresis force is present in both DC and AC electric fields, works encompassing combined DC and AC fields, as well as merely DC or AC fields have been published. In 2003, Kumar *et al.* [49] published their findings on the effects of using only DC fields to align carbon nanotubes. They have found that the nanotubes would deposit on only the positive metal electrode and not bridge the gap between two electrodes. They stated that Coulombic force had dominated and that the nanotubes were negatively charged since they were attracted to the positive electrode [49].

In 2007, Wang *et al.* [45] reported the alignment behavior of ZnO nanowires suspended in ethanol using DC, AC, and both fields combined. Their findings showed that with the source grounded and a 10V DC voltage applied to the drain, the deposition of nanowires shifted from source to drain as gate voltage increased from 0 to 10 V. No explanation was provided as to why this phenomenon occurred. Also, the same group demonstrated a method in which an AC voltage of $15V_{pp}$ was supplied to the Drain electrode, while a DC voltage was applied to the Gate electrode. They reported that the nanowires were well trapped and aligned between the electrodes at a gate voltage of -10V [45].

The effect of combined AC and DC fields was also studied by Fan *et al.* in 2008 [46]. Using Au nanowires suspended in DI water, this group found that the nanowires aligned in the direction of the AC electric field, regardless of whether the DC field was parallel or perpendicular to the AC field. Their conclusion was that the

AC electric field controls the orientation of the nanowires rather than the flow direction of nanowires [46].

The majority of work on the dielectrophoresis of nanowires reported thus far has been based on AC electric field. This is perhaps due to earlier findings on carbon nanotubes where the majority of the nanotubes had deposited on the metal electrodes instead of bridging two electrodes [49]. Also, Evoy *et al.* in 2004 [47] had mentioned that AC fields are often preferred to avoid undesired electrochemical reactions between the electrodes and bridging nanowires, which may potentially cause burn out [47]. Observations using only AC fields include (i) increased number of aligned wires with increasing voltage, and (ii) frequency affects the quality of alignment, whereby at higher frequencies, the wires aligned are more uniform and perpendicular to the electrodes [45]. Raychaudhuri *et al.* in 2009 [30] reported that at higher frequencies, nanowires are more inclined to move along the direction of the electric field gradient rather than electric field lines, resulting in the bridging of nanowires between two electrodes, as opposed to deposition on only one electrode [30].

Although work has been carried out to study the effects of different voltages and frequencies on the alignment behavior of nanowires, they still need improvement, as evident from Figures 2.10 (a) and (b). Also, none have reported the method of frequency tuning to remove nonbridging shorter wires or wires that overlap.

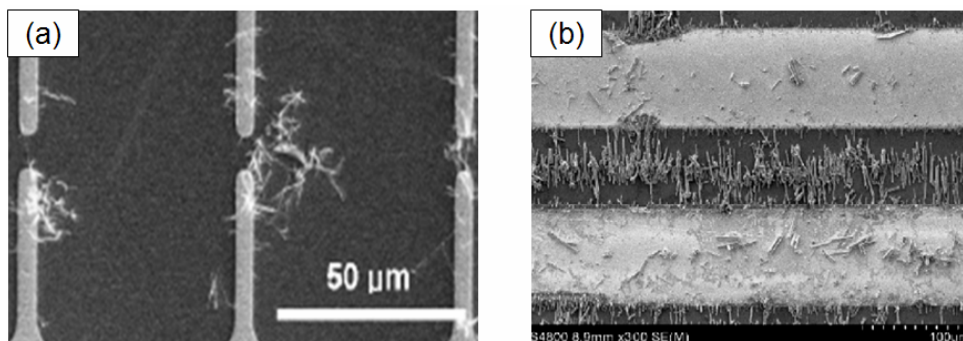


Figure 2.10 Previous results of ZnO nanowire alignment through dielectrophoresis reported by (a) Lee *et al.* [14] (b) Jiang *et al.* [27].

This thesis aims to take a step further in showing how the alignment of nanowires can be improved.

2.4 Conclusion

In this chapter, a review of nanostructures synthesis methods along with their advantages and disadvantages is presented, as well as methods used to characterize the physical, electrical and optical properties of nanostructures.

An introduction to the dielectrophoresis (DEP) theory is also provided. In the interest of nanowires assembly via dielectrophoresis, a closer look into the different forces acting upon nanowires in a microfluidic channel is provided, as well as the effects of conductivity and permittivity of nanowire and medium on the dielectrophoresis force. Several previous works reported on the manipulation of nanowires via dielectrophoresis are also discussed.

3. EXPERIMENTAL TECHNIQUES

This chapter discusses the details of the experiments that have been carried out for the purpose of this research, and entails the methods employed in the synthesis, harvesting, and assembly of ZnO nanowires. In addition, the setup for DC characterization of the nanowires is included.

3.1 ZnO Nanowire Synthesis

The method chosen for the synthesis of ZnO nanowires is the vapor-solid method. Unlike the vapor-liquid-solid method, the vapor-solid method does not require the use of a metal catalyst - a component that poses contamination issues. Also, compared to the hydrothermal method, the vapor-solid method requires shorter growth duration, approximately eight times shorter (1 hour vs. 8 hours).

The vapor-solid method is, in fact, a chemical vapor deposition (CVD) process; thus a basic understanding of its mechanism is fundamental in designing the experiments for nanowire growth. Briefly, the CVD theory states that the mass transport in a reactor chamber is governed by the reactor temperature, pressure, gas flow rate, gas density and reactor geometry [2].

The next subsections describe the characterization of two furnaces that were used for this research.

3.1.1. Lindberg furnace

The Lindberg furnace housed in the Kelley Nanolaboratory is a three-zone furnace. For the purpose of nanowire growth, a cylindrical quartz tube (length ~ 100cm, diameter = 2 inches) attached with an Argon (Ar_2) gas inlet on one end, and a gas purge outlet on the other end is used. Figure 3.1 shows a representation of this system.

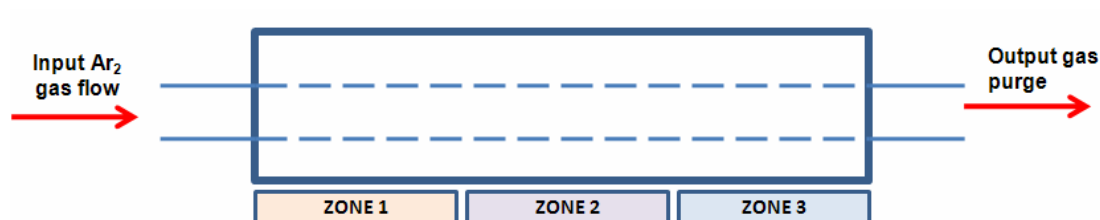


Figure 3.1 A representation of the furnace setup in Kelley Nanolaboratory.

Since temperature plays a major role in CVD process, a study of the temperature profile inside the quartz tube has been carried out. Table 3.1 shows the measured temperature at 35 cm and 45 cm from the left edge of the furnace when different temperature settings were used for Zones 1,2, and 3. A distance of 35 cm from the left edge corresponds to the evaporation region of the source material, while 45 cm corresponds to the deposition/growth region.

Table 3.1 Measured temperatures at 35 cm and 45 cm from the left edge of the Lindberg furnace at different temperature settings for Zones 1,2, and 3.

Zone #	Temperature Setting (°C)					
	Zone 1	940	940	945	955	970
Zone 2	940	940	930	955	970	930
Zone 3	670	720	670	700	720	680
Distance from edge (cm)	Measured Temperature (°C)					
	35	911	911	905	926	944
45	851	855	837	860	878	830

The data from Table 3.1 shows that the deposition region temperature is more dependent upon the setting on Zone 2 rather than Zone 3. A more detailed study was performed for the following settings: Zone 1 = 940°C, Zone 2 = 940°C, and Zone 3 = 670°C, in which temperatures were measured along the furnace at increments of 5 cm. The temperature profile of the furnace at these settings is shown on Figure 3.2.

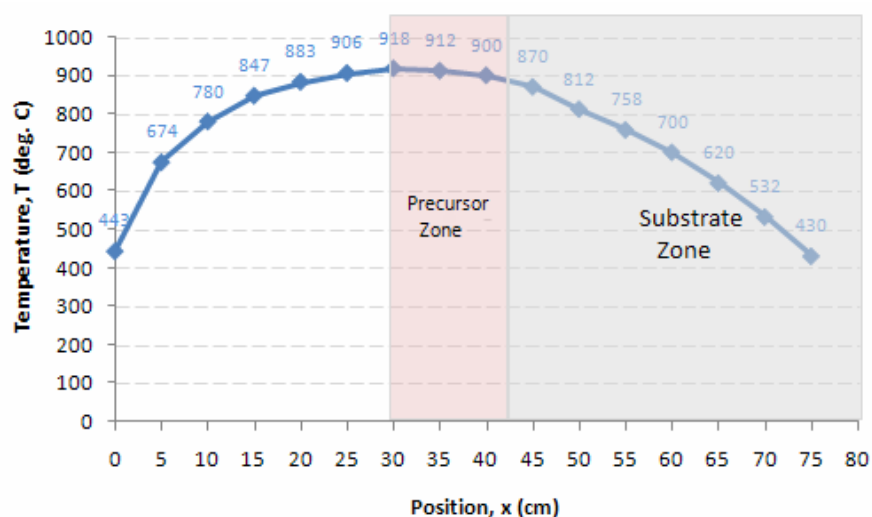


Figure 3.2 Temperature profile of the Lindberg furnace when Zone 1 = 940, Zone 2 = 940 and Zone 3 = 670.

3.1.2. Owen furnace

The furnace that is housed in the Owen clean room is also dedicated for the growth of nanowires. The enhanced features of this second furnace setup include two gas inlets, i.e. for nitrogen (N_2) and oxygen (O_2), and a vacuum system. The oxygen inlet is incorporated to not only introduce the gas but also as a means of controlling the amount desired in the growth chamber. As seen earlier in Equation 2.4, oxygen aids in the nucleation of ZnO nanowires, thus, with better controllability of oxygen and a vacuum system to ensure only the desired gases are present, the process of nanowire growth can be made more reproducible. Figure 3.3 shows the setup for the enhanced furnace.

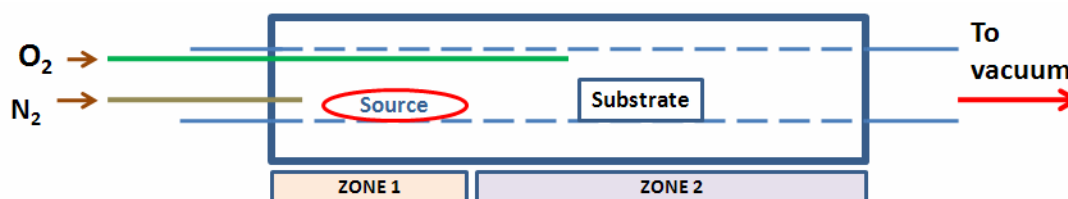


Figure 3.3 A representation of the second furnace setup, whereby an additional O_2 inlet and a vacuum system are incorporated.

3.1.3. Experimental Setup for Nanowire Growth

The source materials used for the growth of ZnO nanowires used for our dielectrophoresis experiment consisted of ZnO powder (Aldrich, 99.99% purity) and graphite powder (Aldrich, 99.99% purity). The ratio for the sources was kept at 1:1 at

0.2 g each. This was also consistent with work reported by several previous groups [64-67].

To ensure an effective carbothermal reaction, the sources were mixed using a quartz pestle and mortar so that they were properly distributed. The substrate used was a Si-substrate with 20 nm of ZnO seed layer [16,68]. The source material was evaporated in the region of the furnace where the temperature was $\sim 920^{\circ}\text{C}$ while the substrate was placed further downstream at $\sim 720^{\circ}\text{C}$. Nitrogen gas was flowed at a rate of 150 sccm to transport the evaporated source material to the deposition region. The growth time employed was 120 minutes. Figure 3.4 gives a representation of the experimental setup. This process yielded nanowires with an average length of $\sim 20\ \mu\text{m}$ and a diameter of $\sim 200\ \mu\text{m}$.

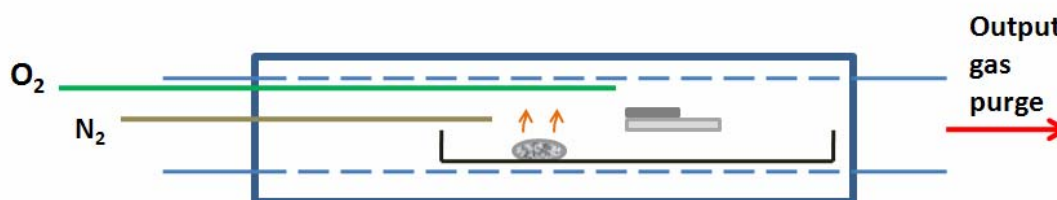


Figure 3.4 The experimental setup for nanowire growth.

3.2 ZnO Nanowire Harvesting

Since the purpose of this research is to study how nanowires can be assembled via dielectrophoresis, it is necessary to have nanowires dispersed in a liquid medium. The most straightforward way to achieve this is by ultrasonically dispersing the ZnO nanowire sample. To ensure a density that is neither too high nor too low, a 2 cm x 2 cm substrate with grown nanowires is submerged in a beaker containing 10 mL of IPA. This assembly is then placed in a Branson 1200 sonicator (120 V, 60 Hz) and sonicated for 1 minute. To determine whether the nanowires are present in the liquid, a small droplet is deposited onto a bare silicon substrate, and viewed under high magnification through an optical microscope. Figure 3.5 shows a representation of the nanowire harvesting process through sonication. The density of nanowires were controlled by making sure parameters such as area of nanowire substrate to be harvested, IPA volume as well as sonication time were the same each time sonication is performed. Also, the nanowire solution is stirred with a magnetic stirrer for about 10 minutes at 800 rpm before an experiment is carried out to ensure homogeneous distribution of nanowire.

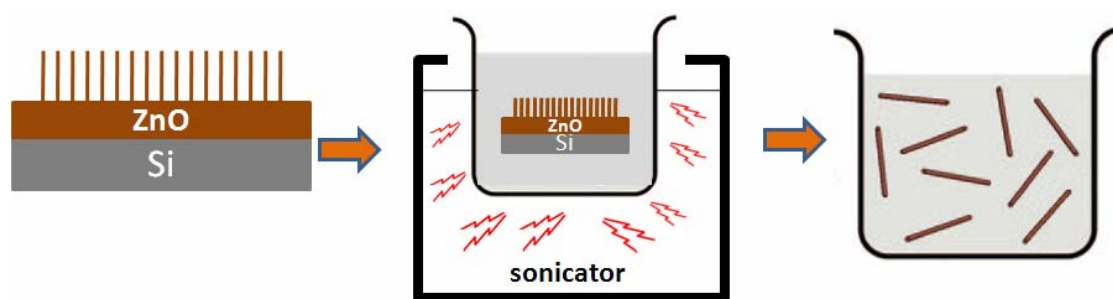


Figure 3.5 Sonication process for harvesting ZnO nanowires from a substrate.

3.3 Dielectrophoresis of ZnO Nanowires

Unlike growing nanobridges, integrating nanowires through dielectrophoresis is advantageous in that it allows the use of a wider range of materials, is cost-effective and requires simple setup [22]. Several preparations are required before the dielectrophoresis experiment can be conducted. The following subsections discuss the work that has been carried out in preparing the substrate, followed by the experimental setup for dielectrophoresis and DC characterization.

3.3.1 Electrode Design

The substrate for dielectrophoresis was designed to have electrode fingers connected to a larger contact pad on each side of the substrate. The aim was to have nanowires aligned in the gap between two opposing electrode fingers. Four gaps were designed, i.e. 2 μm , 5 μm , 8 μm , and 11 μm , in order to align nanowires with lengths close to the designed gaps. According to Zhao *et al.*[42], the DEP force reaches its maximum when the gap size to nanowire length ratio is between 0.85 – 1. Therefore, the multi-gap design within one substrate acts as a ‘filter’ for different nanowire lengths in a solution.

In addition, three ‘trapping’ electrode widths were incorporated in each of the gap, i.e. 0.2 mm, 0.5 mm, and 0.8 mm. This is to verify whether electrode widths would affect the yield of aligned nanowires.

Relative to other dimensions on the electrode substrate, the four gaps were designed to have the smallest gaps in between to two contacts. This is to ensure that the highest electric fields would occur between these gaps, thus optimizing the DEP force, since according to Equation 2.7, F_{DEP} is proportional to the electric field magnitude. The layout for the electrode design was drawn in AutoCAD 2009. Figure 3.6 shows this layout, along with all critical dimensions.

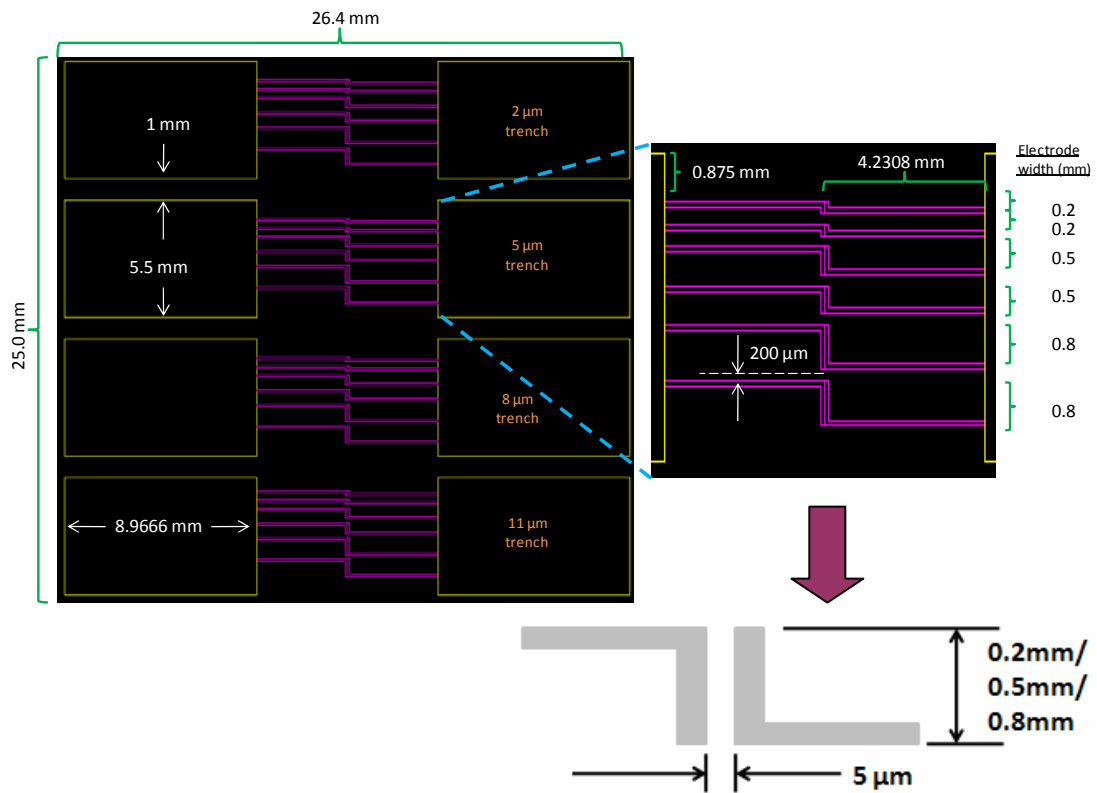


Figure 3.6 The layout of the substrate used for dielectrophoresis experiment.

3.3.2 Fabrication of Substrate

Conventional photolithography and processing steps were carried out in fabricating the structure for the electrode design. However, since the smallest feature was the 2 μm gap, a chrome mask had to be used instead of the typical Mylar mask. With the DWL 66FS Heidelberg housed in the Owen cleanroom, a Chrome mask incorporating the design shown in Figure 3.6 was patterned – a process which consumed ~ 7.5 hours. After the mask was patterned, a series of processing steps were needed in order for the design to be revealed on the chrome substrate.

Before transferring the pattern from the chrome mask, a substrate consisting of a 1 x 1 inch Si-SiO₂ (SiO₂ thickness = 100 nm) deposited with aluminum (Al) was prepared. The aluminum layer was deposited via thermal evaporation using the Polaron Thermal Evaporator in the Owen Cleanroom. Two V-shaped aluminum clips were used to result in an aluminum layer with thickness of $\sim 250\text{-}300$ nm. Although gold (Au) is commonly used as a metal contact, the decision to use Al instead was based on the fact that the barrier height formed between ZnO-Al is 0.05 eV lower than ZnO-Au junction. Since almost all metal-semiconductor junctions will exhibit some rectifying behavior, using Al instead of Au might provide a more Ohmic contact, since the lower the barrier height, the more Ohmic the junction is [69].

A layer of positive photoresist (Shipley 1805) was spun on the aluminum layer as a sacrificial layer during the UV exposure process. The photoresist is less soluble in the developer on areas not exposed to UV. This ensures that the desired

metal contacts are protected during the development of photoresist and subsequently during etching. Type A etchant (80 wt% Phosphoric Acid, 5% Acetic Acid, 5% Nitric, 10% Distilled Water) heated to 90 °C was used to remove unwanted Al regions. The etching process took ~28-35 s.

3.3.3 Experimental Setup for Dielectrophoresis

The setup for dielectrophoresis experiment plays an important role. Two cost effective setups were proposed and investigated:

1. Injecting nanowire solution onto a narrow channel of a tilted patterned substrate
2. Dipping patterned substrate into a nanowire solution

In the first method, a narrow channel (~4mm) was created by placing two long rectangular silicon pieces (25mm x 2mm) on the patterned substrate, to form a channel in the middle, thereby limiting the area of nanowire flow. This would ensure that the nanowires were directed in the area of interest, i.e. the gaps. In addition, the substrate that had been connected to the voltage source was placed on a tilted microscope stage to induce a natural solution flow, so that the nanowires would be able to traverse each gap. The nanowires were deposited on the channel by injecting a volume of 25 μL solution from a 25 μL syringe. Figure 3.7 represents the setup for Method 1.

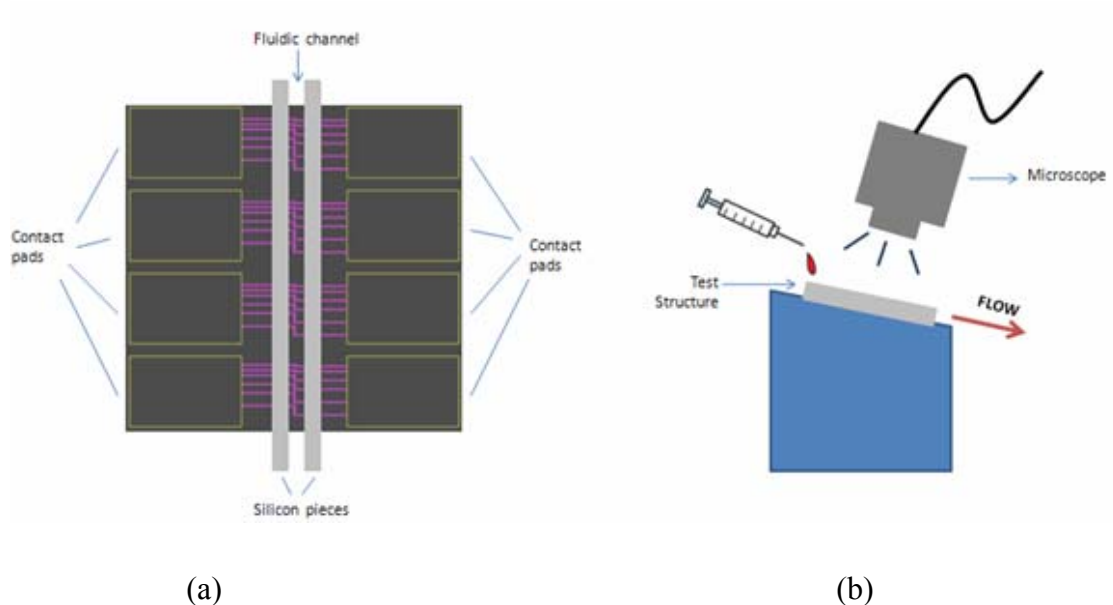


Figure 3.7 Experimental setup for Method 1 : (a) Narrow channel created with long rectangular silicon pieces (b) Tilted substrate for nanowire solution flow.

In Method 2, the patterned substrate was connected to the voltage source and dipped into a nanowire solution, followed by pulling out the substrate so that the alignment of the nanowires can be assisted through capillary force. Also, for optimized alignment, it is important to dip and pull out the substrate in the direction of the desired alignment. Clearly, this method not only utilizes dielectrophoresis force but also benefits from the strong surface tension induced from capillary force. Figure 3.8 is a representation of the setup for Method 2. This setup was built by Josh Triska, a graduate student from the Materials and Devices group of OSU EECS department. Parameters such as lift rate, number of cycles, and delay time can be controlled from this setup. For our experiments, the lift rate was 1 mm/s, number of cycle was 1, and

the delay time was 3 minutes. The delay time refers to the total time the substrate is kept immersed in the solution.

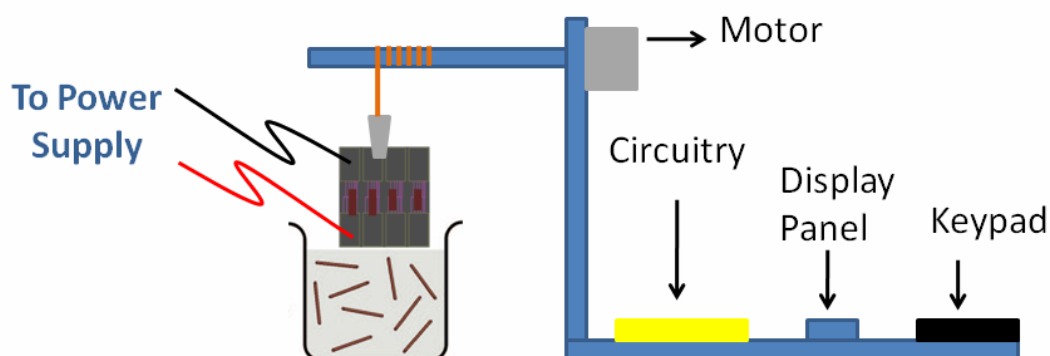


Figure 3.8 Experimental setup for Method 2 [70] – alignment of nanowires through dielectrophoresis force and capillary force.

3.3.4 DC Characterization

Finally, after the nanowires have been optimally aligned in the gaps of the patterned substrate, DC characterization was carried out to study the I-V characteristics of the ZnO nanowires as well as their UV photoresponse.

3.4 Conclusion

In summary, Chapter 3 discusses the experimental techniques employed in fabricating ZnO nanowires, followed by nanowire harvesting and complete details of the dielectrophoresis experiment. For the latter, the layout of the substrate design with critical dimensions has been included. Two experimental setups for dielectrophoresis have been proposed. The first setup requires injecting nanowire solution onto a tilted substrate while the second setup involves dipping the substrate into the nanowire solution. The findings from these two setups shall be presented in the Chapter 5.

4. PARAMETERS AFFECTING NANOWIRE GROWTH

This chapter focuses on the results based on the design of experiment for nanowire growth. Two types of seed layers were studied, i.e. ZnO and Al₂O₃/ZnO. Based on the results from SEM images, the characteristics of grown nanowires were determined, namely its length and diameter. In addition, growth density was also characterized, albeit through visual inspection of the substrate post vapor-solid growth.

4.1 Design of Experiment

A number of parameters are taken into account in the design of experiment for the growth of ZnO nanowires. For this research, the aim is to have uniformly grown nanowires in the range of 5 – 20 μm in length and 100-300 nm in diameter. Since the nanowires are to be harvested for dielectrophoresis, a good yielding growth, i.e. good growth density is desired. To study the effect of growth time, flow rate and deposition temperature on nanowire growth, only one parameter was varied while the other two were kept constant. The effect of seed layer was also incorporated in the study; with two types of substrates, namely zinc oxide layer with alumina layer underneath (Al₂O₃/ZnO) and just zinc oxide (ZnO) layer, tested simultaneously in every run. The reason for incorporating seed layers was to provide nucleation sites for the growth of ZnO nanowires. The seed layers that were deposited using atomic layer deposition

(ALD) had thicknesses of ~15 nm and ~20 nm for aluminum and zinc oxide respectively.

4.1.1 Effect of Growth Time

Table 4.1 shows the qualitative growth density, length and diameter of ZnO nanowires grown on Al₂O₃/ZnO and ZnO seed layer, at three different growth times, namely, 30, 45 and 60 minutes. For both seed layers, longer growth time resulted in higher density of wires. For the ZnO seed layer runs, the results show that longer growth time resulted in bigger diameter. This could be caused by the transport of more growth species with time, hence the growth of rod-like structures. The length of the nanowires grown on ZnO seed layer at 45 minutes cannot be determined due to difficulty in obtaining side view from SEM imaging.

Table 4.1 The design matrix and results for the study of growth time effect on nanowire growth. Constant parameters employed are: flow rate = 150 sccm, deposition temperature = 850 °C.

Seed Layer	Growth Time (min)	Qualitative Growth Density	Length (μm)	Diameter (nm)
Al ₂ O ₃ /ZnO	30	1	3	75~750
	45	3	3~6	30~240
	60	4	3	200
ZnO	30	2	0.5	50~80
	45	3	n/a	50~100
	60	4	0.5	400~500

4.1.2 Effect of Gas Flow Rate

Another parameter of importance in vapor-solid growth is the flow rate of the transporting gas. The inert gas functions as a transporter of growth species from the evaporation region to the deposition region of the growth furnace. Table 4.2 shows the effect of Ar₂ gas flow rate on nanowire growth. Diameters ranging from 400-500 nm were recorded when 150 sccm (square cubic centimeter) of Ar₂ was used - almost 5 to 8 times larger than when 125 sccm of gas was flowed. This suggested that there were less growth species being transported to the deposition site when 125 sccm was flowed for a setup where the substrate was placed 4 cm downstream from the evaporation region, as detailed in Chapter 3 - hence the smaller diameter.

Also, the results show that nanowires are shorter if their diameters are larger. A similar observation had been reported by Kim *et al.* in 2009 [32], where they posited that thicker nanowires have a reduced growth rate compared to thinner ones due to growth species being supplied via surface diffusion along the sidewalls of the nanowires [67].

Table 4.2 also shows that when Al₂O₃/ZnO seed layer is used, the diameter of the nanowires increase with increasing gas flow rate – similar to findings from ZnO seed layer. Some nanowire lengths and diameters could not be determined due to difficulty in SEM imaging.

Table 4.2 The design matrix and results of flow rate effect on nanowire growth. Constant parameters employed are: growth time = 60 min, deposition temperature = 850 °C.

Seed Layer	Flow Rate (sccm)	Qualitative Growth Density	Length (μm)	Diameter (nm)
$\text{Al}_2\text{O}_3/\text{ZnO}$	125	3	n/a	100 ~ 300
	150	4	2 ~ 3	200
	175	0	n/a	n/a
ZnO	125	3	2 ~ 10	20 ~ 100
	150	4	0.5	400 ~ 500
	175	0	n/a	n/a

4.1.3 Effect of Deposition Temperature

Deposition temperature is crucial in making sure that the gas species condense at the growth site to induce nucleation and subsequent nanowire growth. Experiments were carried out at 830°C, 850°C and 880°C to study the effect of deposition temperature. However, the length and diameter of wires were not determined since SEM imaging was not performed. This is because visually the substrates showed either no growth or very thick growth – either case is non-ideal. Nevertheless, the correlation on growth density vs. deposition temperature will be rendered in the upcoming subsection.

Table 4.3 The design matrix and results of deposition temperature effect on nanowire growth. Constant parameters employed are: growth time = 60 min, flow rate = 150 sccm.

Seed Layer	Deposition Temperature (°C)	Qualitative Growth Density
Al ₂ O ₃ /ZnO	830	0
	850	4
	880	4
ZnO	830	0
	850	4
	880	4

4.2 Qualitative Density of Nanowires

Judging by the color of the film on the substrate, growth density was qualitatively assigned by numbers 0 (no growth), 1 (sparse growth), 2 (medium growth), 3 (thick growth) and 4 (very thick growth). Generally, the substrate will appear shiny, almost the same as before it was used for growth, if there was zero to sparse growth. For medium growth, the deposited layer appears bluish; while for thick growth, the film is bluish-grey. For very thick growth cases, the film will appear white. Figure 4.1 gives a summary on the qualitative growth density vs. growth time, flow rate and deposition temperature on both ZnO and Al₂O₃/ZnO seed layers.

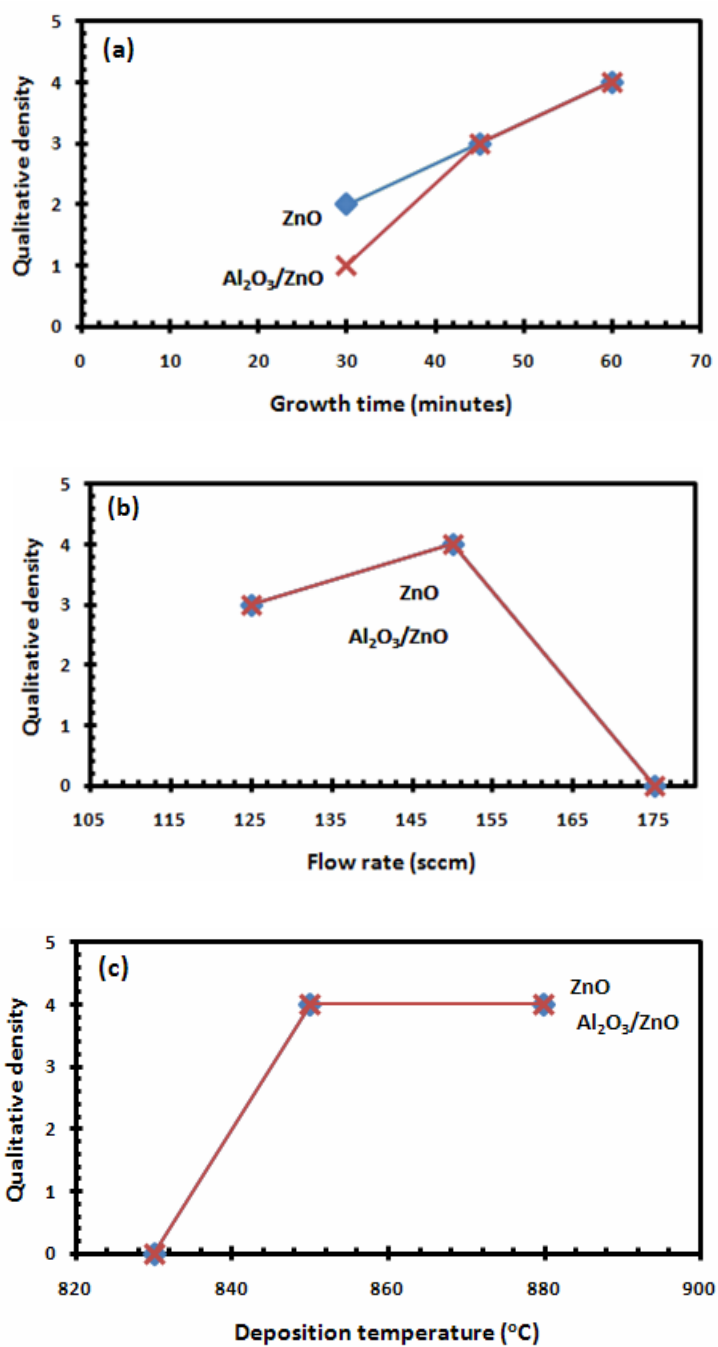


Figure 4.1 Qualitative Growth Density of ZnO nanowires vs. (a) Growth Time – flow rate = 150 sccm, deposition temperature = 850°C (b)Flow Rate – growth time = 60 minutes, deposition temperature = 850°C and (c) Deposition Temperature – growth time = 60 minutes, flow rate = 150 sccm, on ZnO and Al₂O₃/ZnO seed layers

Figure 4.1 (a) show that regardless of the seed layer type, growth density increases with growth time. With increasing growth time, more growth species are delivered to the growth site, hence a thicker growth. In Figure 4.1 (b), the fact that the growth density is higher with 150 sccm of Ar₂ gas flow compared to 125 sccm or 175 sccm shows that the optimized gas flow rate for our experimental setup is at 150 sccm. When the gas flow rate is either too high or too low, the gas species is transported to regions where the substrate is not present, hence the lack in growth density.

Visual inspection showed that there was no nanowire growth when the deposition temperature was set to 830°C. However, when 850°C was utilized, the substrate appeared bluish-grey, and its SEM image showed a highly ordered and dense array of nanowires measuring ~3 μm, as evident from Figure 4.2.

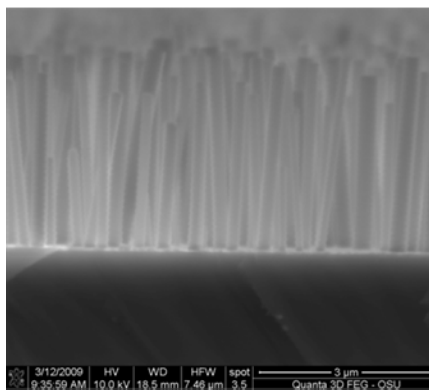


Figure 4.2 SEM image of ZnO nanowires grown on Al₂O₃/ZnO seed layer. (Growth time = 60 minutes, flow rate = 150 sccm, deposition temperature = 850°C)

When the deposition temperature was further increased to 880°C, the substrate appeared white. This could suggest larger grains of ZnO, perhaps even a film of ZnO instead of nanowires since ZnO powder itself is white. Therefore, SEM imaging was not performed for this case.

This correlation study not only provided an insight on the growth behavior and morphology of nanowires but also in optimizing the parameters for our experimental setup. The optimized parameters for high density and well-aligned ZnO nanowires were found by using Al₂O₃/ZnO seed layer, growth time of 60 minutes, Ar₂ flow rate of 150 sccm and deposition temperature at 850°C.

4.3 Conclusion

In this chapter, the parameters affecting nanowire growth have been discussed. These parameters include growth time, gas flow rate and deposition temperature. The optimized parameters for high density and well-aligned ZnO nanowires were found by using Al₂O₃/ZnO seed layer, growth time of 60 minutes, Ar₂ flow rate of 150 sccm and deposition temperature at 850°C. Results in terms of qualitative nanowire density assigned by numbers 0 to 4 as well as the lengths and diameters of the grown nanowires based on a simple design of experiment are also mentioned.

5. NANOWIRE ALIGNMENT VIA DIELECTROPHORESIS

This chapter discusses our experimental findings on nanowire alignment based on applying different biases, varying frequencies, various electrode widths and the two setup methods as introduced in Chapter 3. The removal of shorter wires and overlapping nanowires will be discussed, since our motivation is to eliminate shorter wires that are simply leaking current, and to achieve more uniform device electrical performance by removing overlapping nanowires. The physical and electrical characterization of nanowires aligned through optimized parameters will be discussed as well.

5.1 Effect of Bias

To ensure an optimized dielectrophoresis process, different parameters have been experimented with to find the maximum F_{DEP} . According to Equation 2.7, F_{DEP} is proportional to the electric gradient field, therefore, it would be sensible to utilize the highest peak-to-peak voltage that can be generated from the equipment made available for this experiment. One drawback to using too high a voltage would be that smaller particles or shorter wires would be trapped as well. The decision was to use $10V_{pp}$ since it was the maximum capability of the Elenco GF-8026 function generator. However, to study the effect of negative vs. positive voltages on the alignment behavior of the nanowires, two conditions were experimented with, i.e. voltage sweep from -5V to 5V, and 0V to 10V.

Figure 5.1 shows a comparison of the two biases investigated. The results showed that with -5V to 5V, the nanowires aligned between the gaps but with 0V to 10V, the majority of the nanowires deposited on the grounded (negative) side of the electrode and only a few would bridge the gaps. Figure 5.1 (b) suggests that when 0V to 10V is employed, the electric field is higher at the negative electrode rather than in between the two electrodes. This is because in the positive DEP phenomena – which is the case for our experiment, particles would move towards the region of higher electric field. A similar finding where carbon nanotubes had deposited on the electrodes rather than bridging the electrode gaps was reported by Kumar *et al.* in 2003 [24]. In their experiment, only DC fields were employed, and the deposition behavior was attributed to the effect of Coulombic force [49].

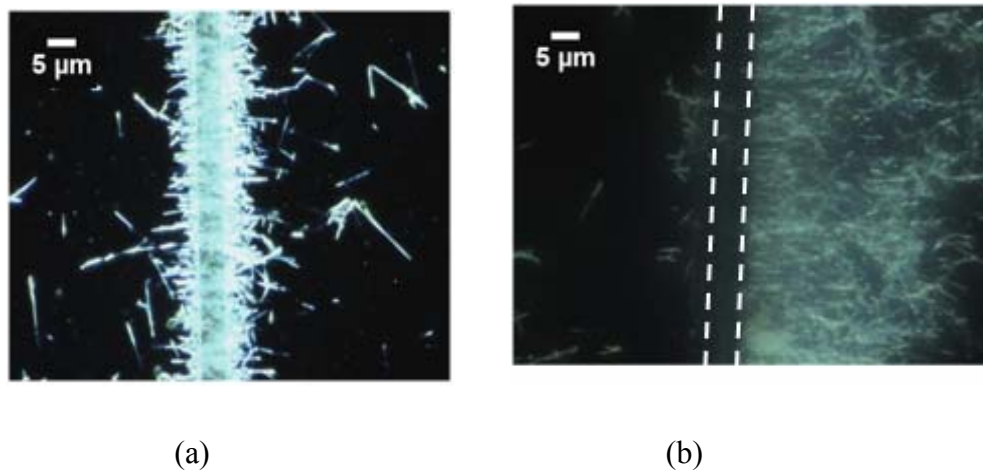


Figure 5.1 Dark field optical microscope images showing the effect of bias on nanowire deposition : (a) -5V to 5V (b) 0V to 10V (Frequency = 10 kHz, nanowire solution volume = 125 μL, gap = 5 μm).

Since our goal is to align nanowires within the gap and not on the electrodes, we decided to use -5V to 5V for our dielectrophoresis experiment.

5.2 Effect of Frequency

To verify the predicted frequency dependence (as shown in Chapter 3) of dielectrophoresis force acting on ZnO nanowires suspended in IPA, experiments at several frequencies were conducted, with -5V to 5V AC voltage applied. The average nanowire length in the solution used for this experiment was around 2 – 5 μm . This is determined by taking the average length measurements of ~350 nanowires, measured by ImageJ software from dark field optical images captured. Figure 5.2 shows the dark field images of nanowires attracted at the electrode gaps of a 5 μm gap.

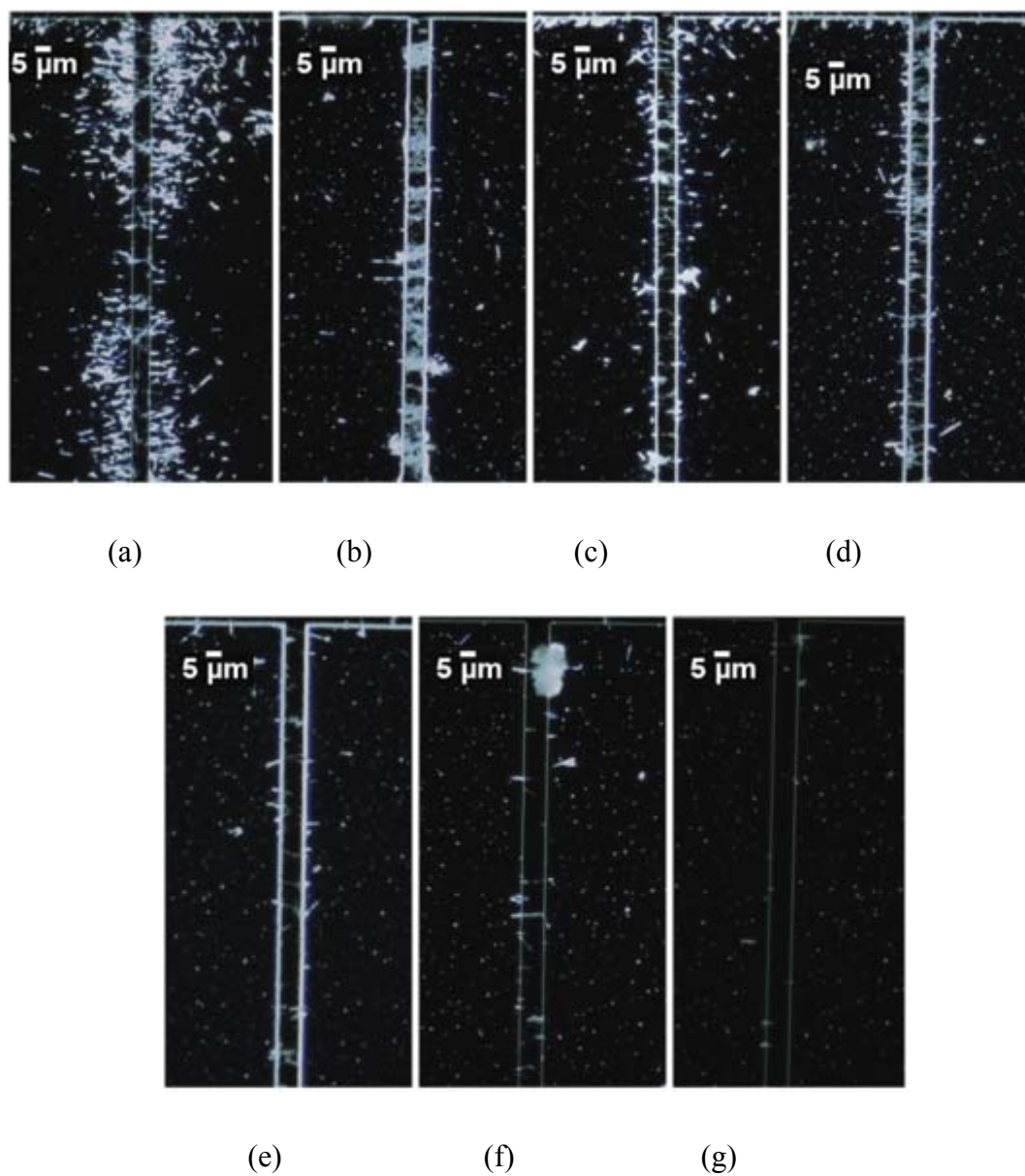


Figure 5.2 Dark field images of nanowires aligned at $10 V_{pp}$ and varying frequencies: (a) 10 Hz (b) 100 Hz (c) 1 kHz (d) 10 kHz (e) 100 kHz (f) 200 kHz (g) 1 MHz.

From these images, it appears that there is a significant decrease in the number of wires aligned from 10 kHz to 100 kHz. This is consistent with the findings reported by Kumar *et al.* and Lee *et al.* in 2009 [48].

At the low frequency of 10 Hz, although many wires were attracted, the majority seem to deposit on the electrodes instead of within the gap. Raychaudhuri *et al.* [30] in 2009 postulated that at low frequencies, nanowires are more inclined to move along the electric field lines instead of the gradient direction and therefore are more likely to be drawn to the electrodes rather than bridging the gap.

Using the ImageJ software, the number of wires and average angle of alignment were extracted from these images for all seven frequencies. Figure 5.3 gives a representation of number of wires versus degree of alignment at various frequencies. At higher frequencies, the degree of alignment is better although the number of wires attracted is less. Since individually bridging rather than overlapping nanowires is desired, a lower angle of alignment is favored because this translates into lower probability of wires crossing one another. In addition, the number of wires is also crucial in ensuring uniform conduction. From our experiments, 10 kHz is chosen as the best setup since at this frequency, the number of wires (~63 wires/mm) is comparable to the number of wires at 1 kHz (~70 wires/mm). Also, 10 kHz is favored over 1 kHz since the angle of alignment measured is lower at 8 degrees as opposed to 11 degrees.

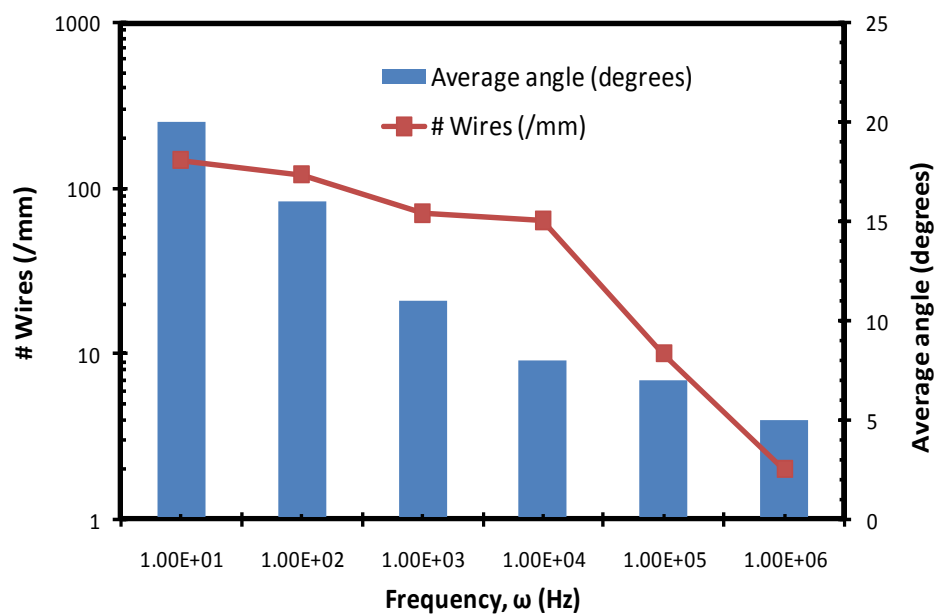


Figure 5.3 Number of wires attracted and average angle of alignment at various frequencies ($V_{pp} = 10$ V).

5.3 Effect of Electrode Width

As shown in Figure 3.6, we incorporated three widths, i.e. 0.2 mm, 0.5 mm, and 0.8 mm for our electrode design. Our results show that there is no correlation between the quality of alignment against width, and that the wider electrode only provides more area for nanowire trapping.

5.4 Effect of Setup

As outlined in Section 3.3.3, two experimental approaches were investigated. Briefly, in Setup 1, nanowire solution is injected onto a narrow channel of a substrate placed on a tilted microscope (~10 degrees tilt). In Setup 2, the entire substrate is dipped and pulled out of a nanowire solution, in a vertical motion.

The results show that in the first setup, more wires were deposited downstream. This could be attributed to a higher drag force on the nanowires due to the tilt, which in turn caused more wires to be delivered and settled downstream. The distance between aligned nanowires for this setup is quite irregular. The separation distance range measured was 67 μm .

In the second setup, the distribution of nanowires is more uniform in every pair of electrodes. Compared to the first setup, the separation distance range measured for the second setup was much smaller at 24 μm . The average distance between two adjacent wires aligned using the second setup was ~10 μm . Figure 5.4 gives a visual representation of the difference in nanowire distribution between the two setups. Therefore, to achieve a more equal distribution of nanowires, which also translates into more uniform devices, Setup 2 appears to be a better choice.

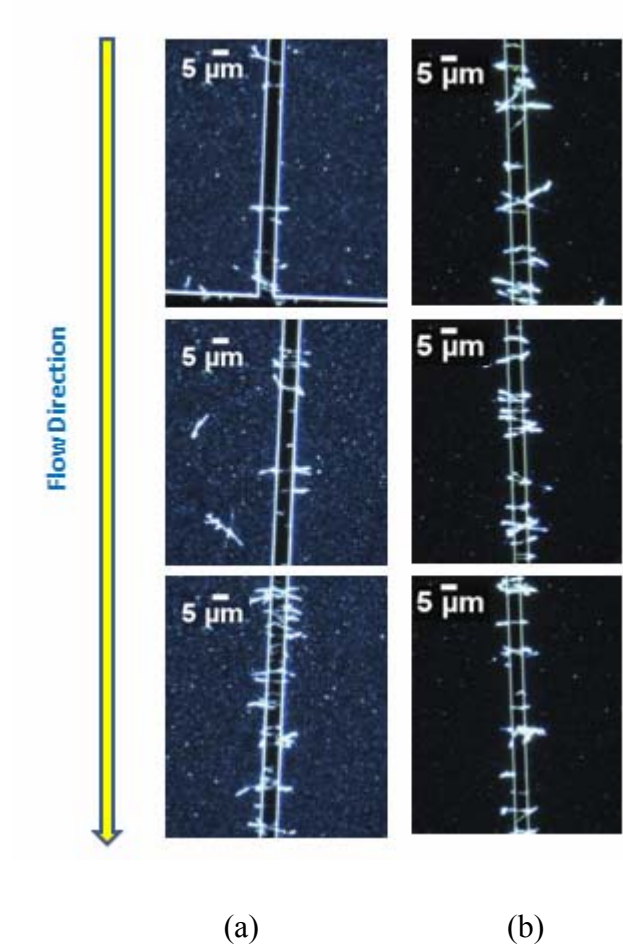


Figure 5.4 Comparison of nanowire distribution between (a) Setup 1 and (b) Setup 2, on a $5\ \mu\text{m}$ gap.

5.5 Removal of Excess Nanowires

A way to reduce nonbridging or overlapping nanowires is by controlling the length and amount of nanowires in a solution. However, this method can be extremely challenging since sonication can cause nanowires to be broken into differing lengths especially if the sonicator power cannot be controlled. Therefore, another method has been investigated, whereby the overlapping nanowires were removed by means of IPA flush and frequency tuning. In this method, experimental setup 2 was utilized, where the lift rate was 1 mm/s, number of cycle was 1 for both the alignment and flushing steps, and the delay time was 3 minutes. Delay time refers to the total time the substrate is kept immersed in the nanowire solution.

We assumed that the overlapping wires have a lesser dielectrophoretic force compared to the ones that are contacted on the electrodes. By tuning the frequency higher (10 kHz to 100 kHz) after alignment, the dielectrophoretic force on the overlapping wires would further reduce. Flushing IPA through these weakly bound nanowires at a force strong enough to hold the bridging nanowires but weak enough to release the short and overlapping wires would eventually remove them from the gaps. This concept has shown to be successful. As evident in Figure 5.5, approximately 70% of overlapping wires have been removed, resulting in the deposition of individual nanowires with fairly equal distance of $\sim 5 \mu\text{m}$ from each other.

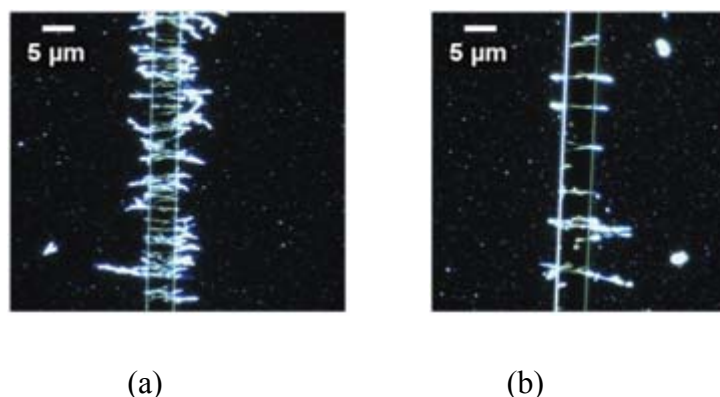


Figure 5.5 Alignment of nanowires at 10Vpp, 10kHz (a) without removal of overlapping nanowires, and (b) with removal of overlapping wires through frequency tuning (10kHz to 100kHz) and IPA flush, on a 5 μ m gap.

In another experiment, the frequency was tuned from 10 kHz to 1 MHz. At 1 MHz, DEP force is further reduced. This has resulted in \sim 95% reduction in nanowires. Compared to flushing at 100 kHz, the separation between aligned nanowires had increased to \sim 20 μ m. These findings are as shown in Figure 5.6. Therefore, 1 MHz might not be the optimum frequency since most wires have been removed.

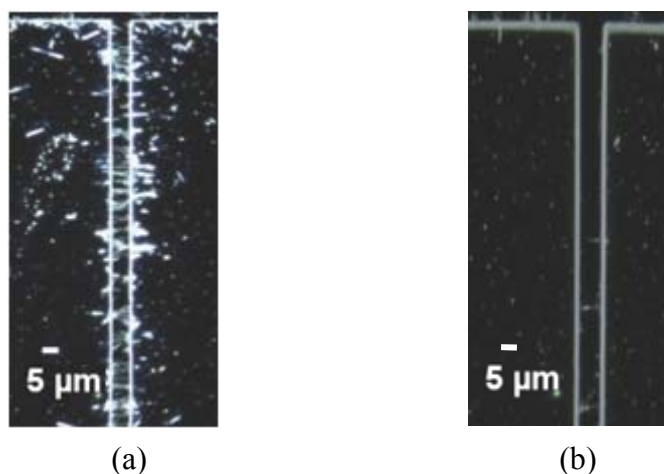


Figure 5.6 Alignment of nanowires at 10Vpp, 10kHz (a) without removal of overlapping nanowires, and (b) with removal of overlapping wires through frequency tuning (10kHz to 1 MHz) and IPA flush, on a 5 μ m gap.

Additional images from the nanowire removal experiments through frequency tuning at 1 kHz – 100 kHz, 1 kHz – 200 kHz, and 1 kHz – 1 MHz can be found in Appendix A.

5.6 Conclusion

This chapter discusses the important factors that need to be taken into account in optimizing the dielectrophoresis experiments. They include bias, frequency, and experimental setup. Experiments carried out to find the optimized settings for each of these factors were presented. The best settings were -5 V to 5 V applied bias at 10 kHz and experimental Setup 2, which had resulted in higher yielding and better degree of nanowire alignment within the gap, as well as more equally distributed nanowires across the electrodes. Excess or overlapping nanowires have been successfully removed via flushing with IPA post alignment at a higher frequency of 100 kHz, as shown in Figure 5.5.

6. ELECTRICAL AND PHOTORESPONSE MEASUREMENTS

This chapter discusses the electrical measurements as well as the photoresponse measurements performed on the ZnO nanowires that have been aligned dielectrophoretically using optimized parameters detailed in the previous chapter.

6.1 Electrical Measurements

Current-Voltage (I-V) measurements were performed on the dielectrophoretically-aligned ZnO nanowires for electrical characterization. Measurements were taken pre- and post top contact deposition. Since without any top contacts only the bottom portion on two ends of the nanowires are contacted to the metal electrodes, we anticipated poor conduction. However, the advantage of DEP is that we can lithographically align contacts to the nanowires. Therefore, we deposited ~150 nm of aluminum and performed liftoff in acetone to form the top contact. Figure 6.1 gives a representation of the pre- and post top contact deposition. The top metal contacts measured 0.5 mm x 0.05 mm, and were aligned to cover 1 μm inward on each side of the original 5 μm gap, resulting in a 3 μm final separation. This is to ensure good coverage of the nanowires, especially the ones that are only slightly touching the edge of the bottom contact.

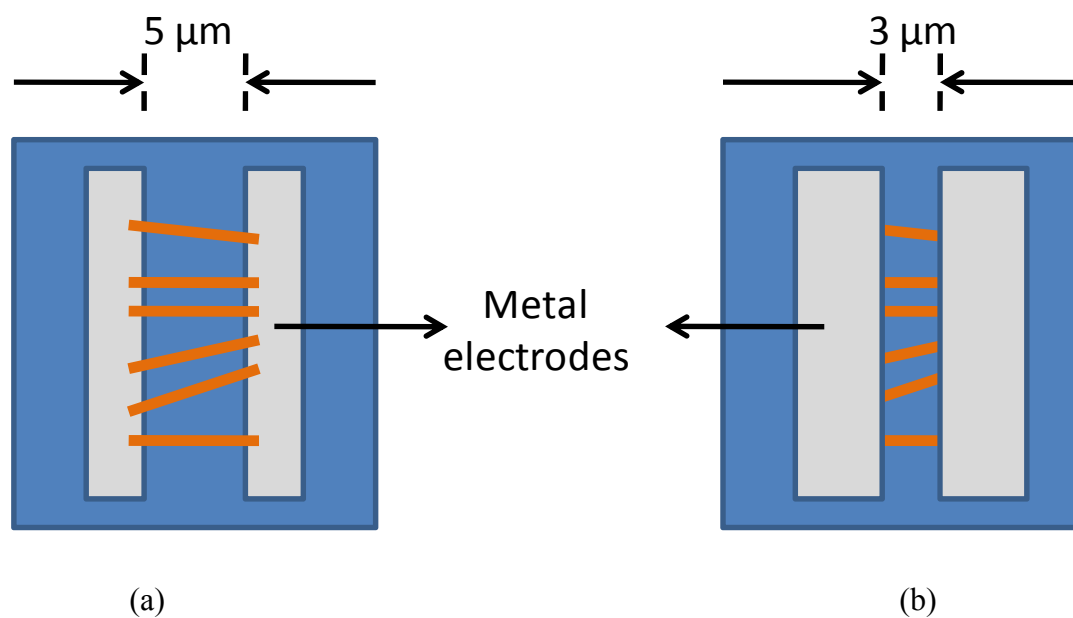


Figure 6.1 Representation of dielectrophoretically-aligned nanowires (a) on bottom metal contacts and (b) with additional top metal contacts.

Sonication had to be performed to selectively liftoff the top aluminum layer so that the top contacts would not be shorted. The sonication time was ~ 10 s. Although aluminum within the 3 μm gap was successfully removed, about 50% of the underlying bridging wires were removed in the process. Figure 6.2 shows the difference in the number of wires before and after sonication process.

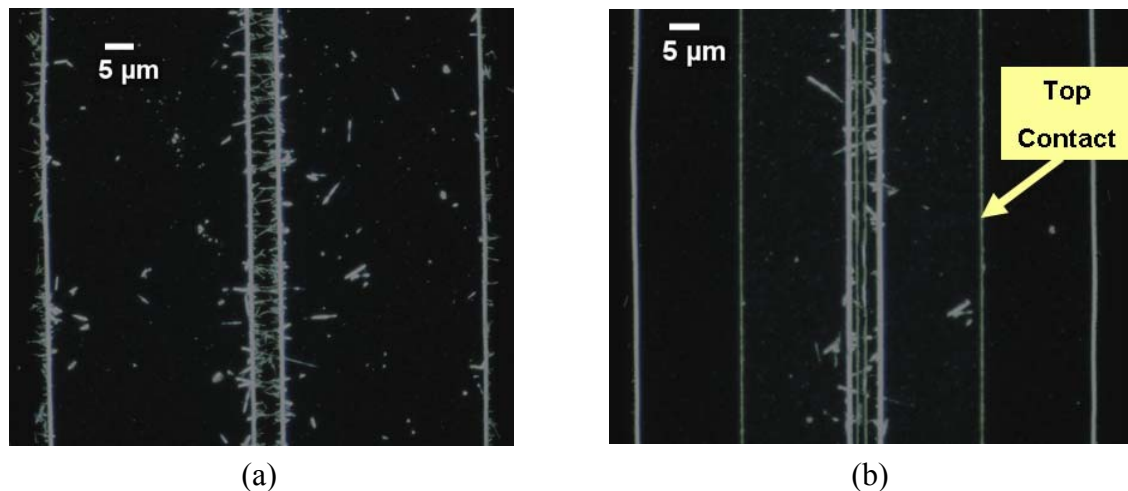


Figure 6.2 A comparison of number of aligned/bridging nanowires (a) before sonication (b) after 10 seconds sonication on a 0.2 mm long, 5 μm wide gap.

I-V measurements on the aligned nanowires were performed using the Agilent 4155C Semiconductor Parameter Analyzer. In comparing the electrical behavior for pre- and post top contact, current was plotted against normalized E-field instead of the voltage. This would give a more accurate comparison since E-field is proportional to voltage but inversely proportional to distance ($E = V/d$). Drain-source voltage, V_d , of -15V to 15V was employed. For bottom and top contacts, the distances used for E-field calculation was 5 μm and 3 μm respectively.

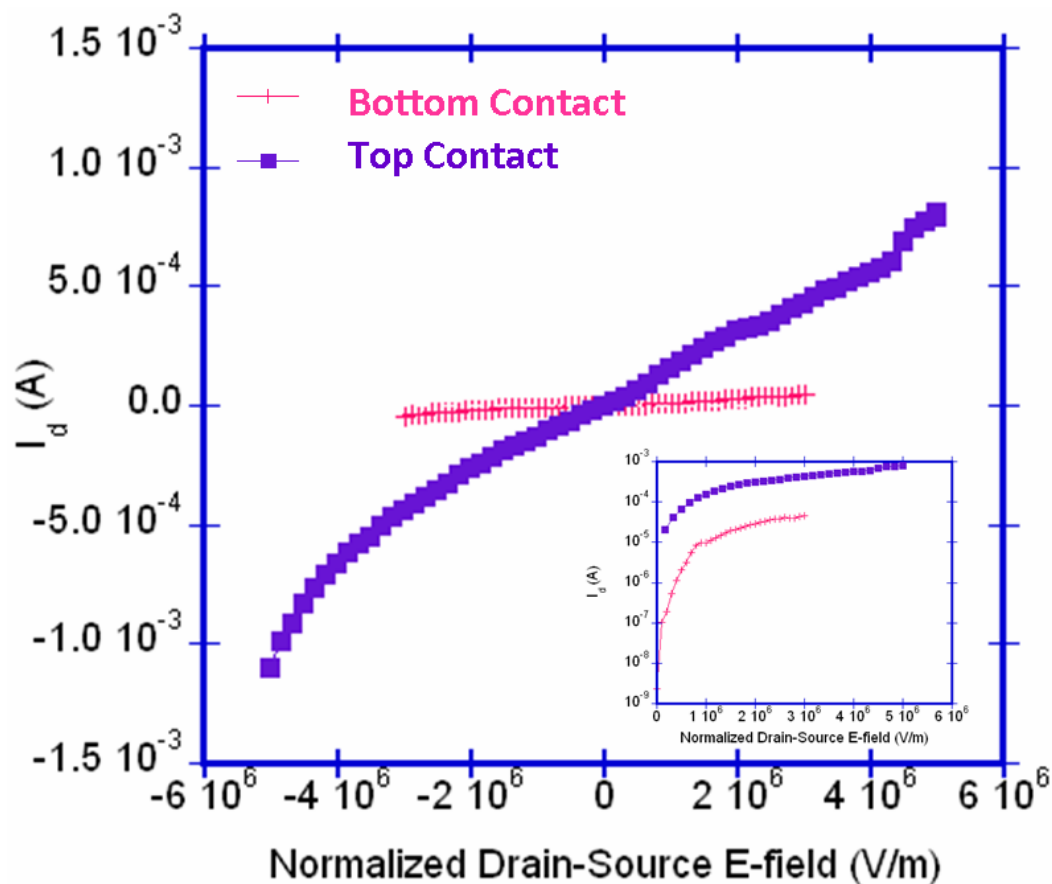


Figure 6.3 A comparison of current vs. normalized E-field behavior of dielectrophoretically aligned ZnO nanowires with only bottom contact, and with additional top contact. (inset) - data in log scale.

As seen in Figure 6.3, the measured drain current, I_d with just bottom contacts is minimal. However, with the addition of top contacts, a linear ‘Ohmic’ curve was observed, with the maximum current measuring 4.9×10^{-4} A at 3.0×10^6 V/m - approximately one order of magnitude higher than without top contacts. Also, the conductance with top contacts was measured to be about 0.15 nS. However, the measured leakage current from the back gate, I_g , post top-contact was quite high, \sim

0.25 mA maximum when a voltage of 5×10^6 V/m is applied across the source and drain electrodes. Although the cause of the leakage was not determined, one possible leakage path between the drain-source electrodes is through the SiO_2 , as shown in Figure 6.4.

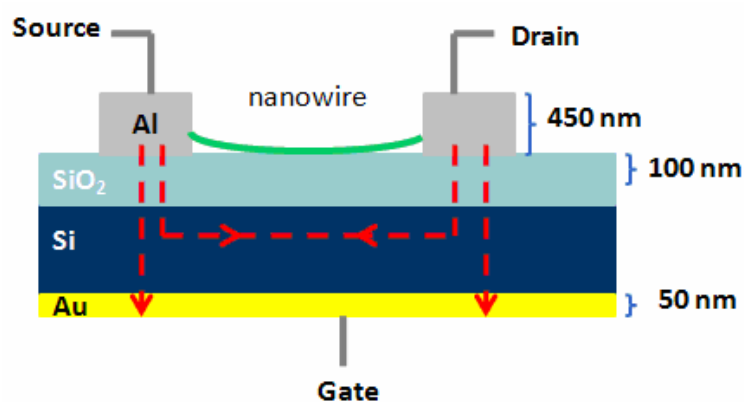


Figure 6.4 Possible current leakage path in a MOSFET device.

Although 1.5 MV/cm is well below the typical breakdown strength for thermally grown SiO_2 , the SiO_2 has been subjected to ~ 1 MV/cm AC stressing in an aqueous environment which may result in a more leaky film.

Scratches on the aluminum electrodes surface due to contact pins used during dielectrophoresis experiment or tungsten tips used in probing for electrical measurements could have resulted in mechanical stressing of the SiO_2 . The stress induced during both of these processes could have contributed to increased leakage paths in the SiO_2 layer.

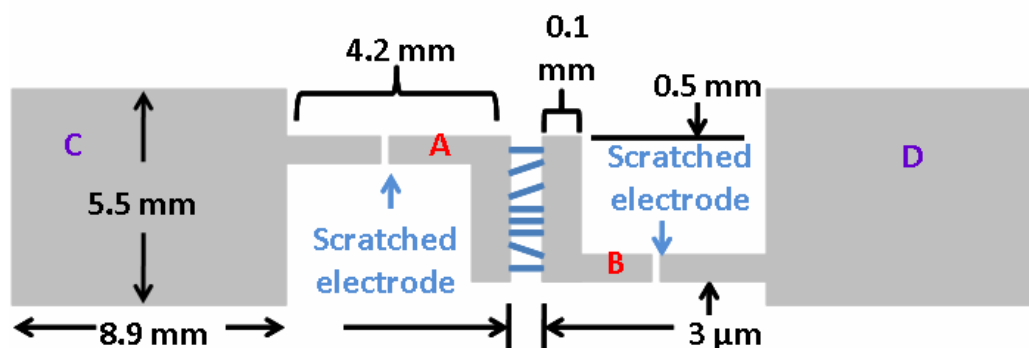


Figure 6.5 Diagram showing scratched electrodes and points A and B where probing was performed (instead of at points C and D) to reduce current leakage.

Another reason that might have contributed to high current leakage is the big contact area of the contact pads. To minimize this component, we scratched off the surface of the aluminum electrodes so that the contact area for probing would be smaller. As shown in Figure 6.5, instead of probing at points C and D on the contact pads, we scratched off the electrodes at around the midpoints of their lengths, and probed at points A and B. The contact area reduced by an order of $\sim 24X$. With lesser area, leakage current is reduced.

The leakage current, I_g at every gate voltage applied was simultaneously measured along with drain current, I_d . As seen from Figure 6.6 (a), the leakage currents were small - about four orders of magnitude lower than the measured drain currents shown in Figure 6.6 (b). The leakage current recorded was a little higher at -3 V and gradually stabilizes as V_d progresses because we did not employ any delay time at the start of measurement. We observed the gate voltage (V_g) control whereby V_g

was set to either -10V, 0V, or 10V while the drain-source voltage, V_d was swept from -3V to 3V.

Figure 6.6 (b) shows that gate control was present, though more apparent in the negative region of V_d . The asymmetry of the I-V curve could be attributed to the shift in the top contact alignment. Since a 3 μm feature had to be aligned visually, albeit with alignment marks, we anticipated less than perfect alignment. Therefore, one side of the nanowire might have better top contact than the other, thus causing the asymmetry. Our results showed the highest current modulation at $V_d = -3\text{V}$, between $V_g = 0\text{V}$ and $V_g = -10\text{V}$, where the drain current increased by a factor of 1.2 (shown by arrow in Figure 6.6(b)). Also, the fact that the magnitude of the current decreased when V_g was decreased from 0 V to -10 V indicated n-type behavior of the ZnO nanowires. Work by different groups on ZnO nanowires [14,43] and GaN nanowires [26] have demonstrated gate voltage control as well.

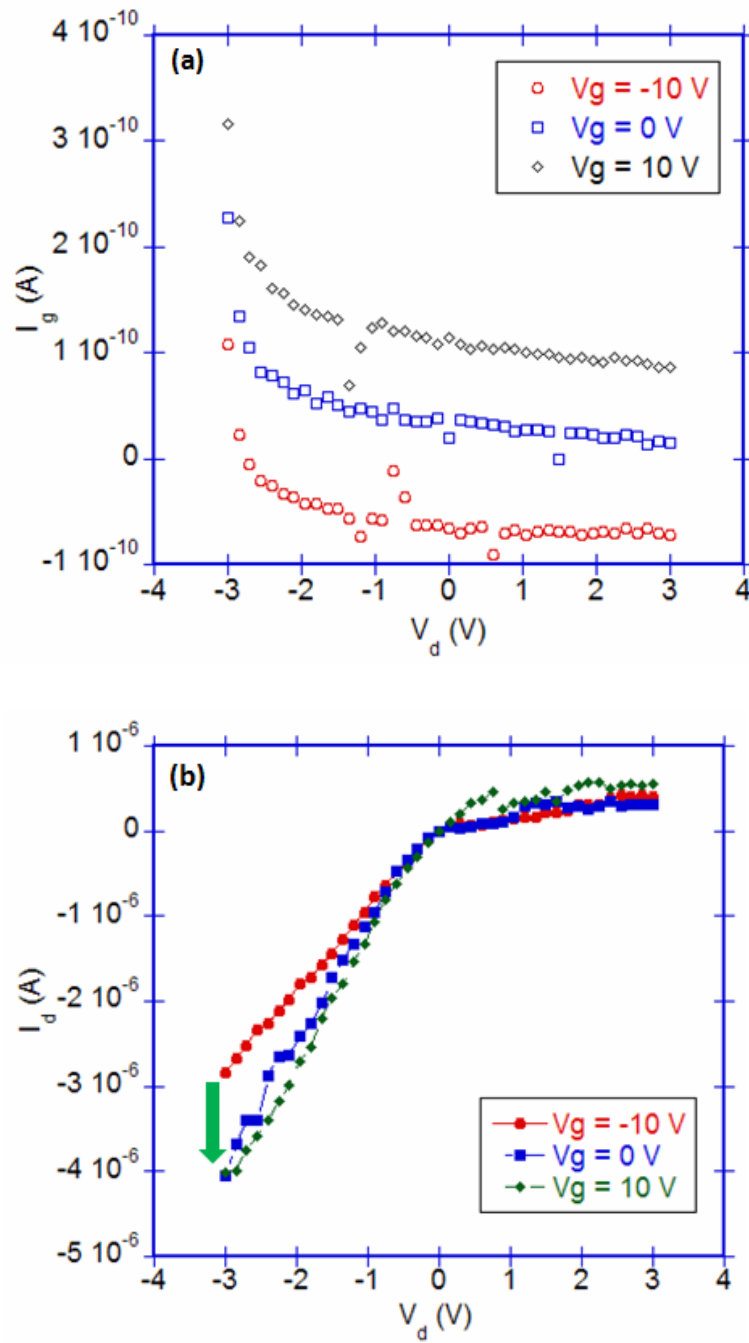


Figure 6.6 I-V measurements showing (a) Leakage current vs. drain voltage (b) Drain current vs. drain voltage, with gate control ($V_g = -10$ V, 0 V, 10 V).

6.2 Photoresponse Measurements

Photoresponse measurements were performed since ZnO nanowires are well known to be sensitive to UV light. Current versus time behavior was measured at an applied V_d bias of 3 V, a 254 nm wavelength, 18.4 W Mineralight UV light source was used, while UV light was pulsed at 30 seconds and subsequently removed for 1 minute before the next pulse. Figure 6.7 shows the results obtained.

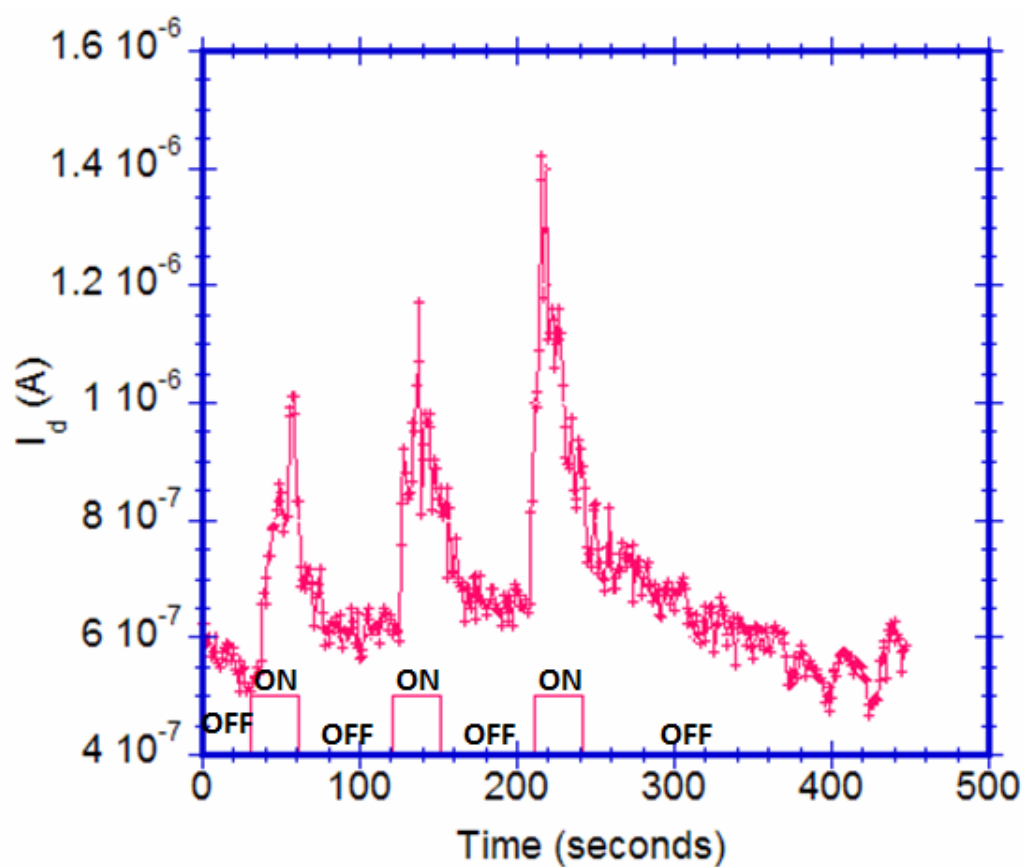


Figure 6.7 Photoresponse obtained by continually switching the UV light on and off at an applied bias of 3 V.

The highest current modulation was observed at the third pulse, where current increased by a factor of 2, with a rise time of ~ 9 seconds. When UV light is radiated, electron-hole pairs are generated in the ZnO nanowires. The holes move to the surface of the nanowire and combine with the oxygen ions through surface electron-hole recombination. As a result, the oxygen molecules are desorbed and the unpaired electrons contribute to higher conductivity [21]. When UV light is switched off, the unpaired electrons would recombine with the oxygen ions, causing oxygen to readsorb onto the surface, thus reducing conductivity. Lee *et al.* [21] showed two orders of magnitude increase in their photoresponse measurement of dielectrophoretically-aligned ZnO nanowires. The discrepancy between their results and ours could be due to several reasons. The photoresponse reported by Lee *et al.* [21] was that of a single ZnO nanowire. This explains their consistent and high on/off current ratio. In our case, we had ~ 50 nanowires and this contributes to variations in the nanowire diameters, resulting in the nonconsistent peak current at each pulse. The calculated length to diameter ratio of the nanowire from Lee *et al.* [21] was 233, about 10 times higher than ours. This translates into higher surface area, thus higher sensitivity since most sensing reactions happen on the surface [2,5]. This explains why their photoresponse is better.

6.3 Conclusion

This chapter presented the I-V characteristics and photoresponse measurements of our dielectrophoretically-aligned ZnO nanowires. The addition of top contacts has shown improved current conduction. Gate control was observed although in an asymmetric pattern. Possible reasons attributing to non-ideal electrical measurements have been discussed. Photoresponse measurements obtained were compared to an earlier reported work, in which likely causes that had led to discrepancies were mentioned.

7. CONCLUSIONS AND FUTURE WORK

7.1 Conclusions

Work on individually constructed devices has demonstrated that nanowires offer great promise for applications such as sensing and optoelectronics. Despite this work, reliable large scale alignment and integration of these individual nanostructures into a lithographically defined process remains a challenge. The motivation for this thesis is to not only align nanowires using dielectrophoresis but also to further improve their alignment through frequency tuning and IPA flushing, since previous works have not shown much improvement on achieving individually-deposited nanowires that translate to more uniform devices.

Although the main focus of this thesis is on the assembly of ZnO nanowires through dielectrophoresis, a complete picture beginning from nanowire synthesis to the various experiments carried out for dielectrophoresis as well as the electrical and photoresponse measurements obtained have been presented.

In nanowire synthesis, the effects of growth time, gas flow rate, and deposition temperature have been studied. We have found that the increase of growth time causes the qualitative density of nanowires to increase. In terms of gas flow rate, an increased density of nanowires was observed from an increase of 125 sccm to 150 sccm. However, when the flow rate is further increased to 175 sccm, the nanowire density plunged to zero. This means that the optimized flow rate is dependent upon the

position of the substrate in the furnace. Our finding on different deposition temperatures shows an increase in nanowire density from 830°C to 850°C. However, there was no difference in density from 850°C to 880°C. Also, the use of an Al₂O₃ layer beneath ZnO improves the orientation of the grown nanowires. This has been attributed to matched lattice constant.

To better understand the role of conductivity and permittivity in dielectrophoresis, we calculated the frequency response of the Clausius-Mossotti factor, $\text{Re}[K(\omega)]$, which is in proportion to the dielectrophoresis force. We found that the drop in dielectrophoresis force occurs at a higher frequency when a higher medium conductivity or a lower medium permittivity is used. A higher nanowire conductivity, on the other hand, increases only the magnitude of the $\text{Re}[K(\omega)]$. The permittivity of nanowire does not alter the magnitude or frequency response of $\text{Re}[K(\omega)]$.

The investigation on the effect of bias shows that at only positive voltages, i.e. 0 V to 10 V, the nanowires tend to deposit on a particular electrode. This finding is somewhat similar to an earlier work on carbon nanotubes which had employed DC fields for dielectrophoresis [49]. Therefore, if we intend to trap nanowires in between two metal electrodes, it would be best to use both the negative and positive voltage range.

In terms of the effects of frequency, we have found that the number of wires reduces significantly beyond 10 kHz, while the degree of alignment improves gradually from 10 Hz to 1 MHz. Therefore, in the interest of yield and alignment

quality, 10 kHz appears to be the best choice. We have also shown that excess or overlapping nanowires can be removed by adjusting the frequency higher while flushing with IPA. 100 kHz is preferred over 1 MHz since at the latter frequency, almost 95% of the initially deposited wires were removed.

For the dielectrophoresis experimental setup, two methods have been investigated. In the first setup where the substrate was tilted while nanowire solution is flowed, our findings show that more wires were attracted downstream, due to the accumulation and longer settling time of the solution. This has resulted in nonuniform distribution of nanowires and would not be a good setup if uniform devices were desired. Therefore, we experimented with another setup where the entire substrate was dipped into and pulled out of the nanowire solution. This method appeared better than the first setup, since the number of aligned nanowires was more uniform on each electrode pair, and that the variation in separation distance was much lower.

To determine whether the dielectrophoretically-aligned nanowires could be used as a device, I-V measurements have been carried out. With a top layer of aluminum deposited on the ends of the nanowires, an Ohmic behavior has resulted, with a measured conductance of 0.15 nS. The nanowires also exhibit gate voltage control, albeit not in a symmetrical way. A reason for this could be the shift in top aluminum contact due to imperfect alignment. Due to this, the top contact could have only covered one end of the nanowire, causing unequal conductivities that might have given rise to the asymmetry behavior. The nanowires have also shown photoresponse, with a factor of 2 increase in current when UV light was radiated.

This research has shown that nanowires can indeed be manipulated by electric field to produce uniform alignment. A method to remove excess or overlapping nanowires through frequency tuning and IPA flush has been shown successful. This method would be beneficial especially when the variation in nanowire length post harvesting is large.

7.2 Future Work

Although the optimum bias and frequencies have been discussed in this thesis, it would be better to use a solution that contains nanowires with more uniform length distribution. This would result in higher yielding bridging nanowires since the number of shorter wires would be reduced. To achieve more uniform nanowire length distribution, a more controlled synthesis method could be employed, followed by the use of a power-controllable sonicator. The latter could lessen the occurrence of broken nanowires.

Since ZnO is an ideal candidate for sensing applications, future work could include the response to oxygen and water vapor at different flow rates and temperatures for the dielectrophoretically-aligned nanowires. Also, a top gate configuration could be looked into to investigate any differences in I-V measurements compared to bottom gate measurements reported in this thesis.

Also, in order to better convey the results from dielectrophoresis experiments, real-time imaging would be beneficial. Perhaps a PDMS microchannel along with flow-rate controlled nanowire solution injection could be employed to aid imaging.

BIBLIOGRAPHY

1. Y. Xia, P. Yang, Y. Wu, Y. Mayers, B. Gates, B. Yin, Y. Kim, F. and H. Yan, "One-Dimensional Nanostructures: Synthesis, Characterization, and Applications," *Advanced Materials*, vol. 15, pp. 353-389, 2003.
2. G. Cao, *Nanostructures and Nanomaterials: Synthesis, Properties & Applications*, Imperial College Press, 2004.
3. Z. L. Wang, "Theme issue: inorganic nanotubes and nanowires," *Journal of Materials Chemistry*, vol.19, pp. 826-827, 2009.
4. L. Schmidt-Mende and J. L. MacManus-Driscoll, "ZnO - nanostructures, defects, and devices," *Materials Today, Elsevier Science Ltd*, vol. 10, pp.40-48, 2007.
5. G. Shen, P. Chen, K. Ryu, and C. Zhou, "Devices and chemical sensing applications of metal oxide nanowires," *Journal Of Materials Chemistry, Royal Soc. Chemistry*, vol. 19, pp. 828-839, 2009.
6. V. La Ferrara, B. Alfano, E. Massera, and G. Di Francia, "Palladium Nanowires Assembly by Dielectrophoresis Investigated as Hydrogen Sensors," *IEEE Transactions On Nanotechnology, IEEE-Inst Electrical Electronics Engineers Inc*, vol. 7, pp. 776-781, 2008.
7. M. Koto, P. W. Leu, and P. C. McIntyre, "Vertical Germanium Nanowire Arrays in Microfluidic Channels for Charged Molecule Detection," *Journal of the Electrochemical Society, Electrochemical Soc. Inc*, vol. 156, pp. K11-K16, 2009.
8. Y. P. Hsieh, M. Hofmann, H. Son, X. Jia, Y. F. Chen, C. T. Liang, M.S. Dresselhaus, and J. Kong, "Direct deposition of single-walled carbon nanotube thin films via electrostatic spray assisted chemical vapor deposition," *Nanotechnology*, vol. 20, 2009.

9. J. Xiang, W. Lu, Y. Hu, Y. Wu, H. Yan, and C. Lieber, "Ge/Si nanowire heterostructures as high-performance field-effect transistors," *Nature*, vol. 441, pp. 489-493, 2006.
10. R.J. Tilley, *Understanding Solids: The Science of Materials*, John Wiley & Sons Ltd, 2004.
11. P. C. Chang and J. G. Lu, "ZnO Nanowire Field-Effect Transistors," *IEEE Transactions on Electron Devices*, vol. 55, pp. 2977-2987, 2008.
12. Z. Gao, J. Zhou, Y. Gu, P. Fei, Y. Hao, G. Bao, and Z. L. Wang, "Effects of piezoelectric potential on the transport characteristics of metal-ZnO nanowire-metal field effect transistor," *Journal Of Applied Physics, American Inst. Physics*, vol. 106, 2009.
13. P. Chang, Z. Fan, D. Wang, W. Tseng, W. Chiou, J. Hong, and J. Lu, "ZnO nanowires synthesized by vapor trapping CVD method," *Chemistry Of Materials, American Chemical Soc.*, vol. 16, pp. 5133-5137, 2004.
14. S. K. Lee, S. Y. Lee, J. H. Hyung, C. O. Jang, D. J. Kim, and D. I. Suh, "AC dielectrophoresis alignment of ZnO nanowires and subsequent use in field-effect transistors," *Journal Of Nanoscience And Nanotechnology*, vol.8, pp. 3473-3477, 2008.
15. J. Kang, S. Myung, B. Kim, D. Oh, G. T. Kim and S. Hong, "Massive assembly of ZnO nanowire-based integrated devices," *Nanotechnology*, vol. 19, 2008.
16. J. F. Conley, Jr., L. Stecker, and Y. Ono, "Selective growth and directed integration of ZnO nanobridge devices on Si substrates without a metal catalyst using a ZnO seed layer," *J. Elec. Mat.*, vol. 35(4), pp. 795-802, 2006.
17. M. Islam, S. Sharma, T. Kamins, and R. Williams, "Ultrahigh-density silicon nanobridges formed between two vertical silicon surfaces," *Nanotechnology*, vol. 15, pp. L5-L8, 2004.
18. J. F. Conley, Jr., L. Stecker, and Y. Ono, "Directed integration of ZnO nanobridge devices on a Si substrate," *Applied Physics Letters*, vol. 87, pp. 223114-223116, 2005.

19. Z. Kang, C. H. A. Tsang, D. D. D. Ma, N. B. Wong, and S. T. Lee, "Nanomaterials separation by an ultrasonic-assisted phase transfer method," *Chemical Physics Letters, Elsevier Science BV*, vol. 455, pp. 252-255, 2008.
20. M. P. Hughes, "Strategies for dielectrophoretic separation in laboratory-on-a-chip systems," *Electrophoresis*, vol. 23, pp. 2569-2582, 2002.
21. S. H. Lee, H. J. Lee, K. Ino, H. Shiku, T. Yao, and T. Matsue, "Microfluid-assisted dielectrophoretic alignment and device characterization of single ZnO wires," *Journal of Physical Chemistry C, American Chemical Society*, vol. 113, pp. 19376-19381, 2009.
22. A. Boccaccini, J. Roether, B. Thomas, M. Shaffer, E. Chavez, E. Stoll, and E. Minay, "The electrophoretic deposition of inorganic nanoscaled materials," *Journal Of The Ceramic Society Of Japan, Ceramic Soc Japan-Nippon Seramikkusu Kyokai*, vol.114, pp.1-14, 2006.
23. A. Motayed, M. He, A.V. Davydov, J. Melngailis, and S. N. Mohammad, "Simple model for dielectrophoretic alignment of gallium nitride nanowires," *Journal of Vacuum Science & Technology B*, vol. 25, pp. 120-123, 2007.
24. M. Kumar, S. Lee, T. Kim, T. Kim, S. Song, J. Yang, K. Nahm, and E. Suh, "DC electric field assisted alignment of carbon nanotubes on metal electrodes," *Solid-State Electronics, Pergamon-Elsevier Science Ltd*, vol. 47, pp. 2075-2080, 2003.
25. J. Suehiro, N. Nakagawa, S. Hidaka, M. Ueda, K. Imasaka, M. Higashihata, T. Okada, and M. Hara, "Dielectrophoretic fabrication and characterization of a ZnO nanowire-based UV photosensor," *Nanotechnology*, vol. 17, pp. 2567-2573, 2006.
26. S. Y. Lee, T. H. Kim, D. I. Suh, N. K. Cho, H. K. Seong, S. W. Jung, H. J. Choi, and S. K. Lee, "A study of dielectrophoretically aligned gallium nitride nanowires in metal electrodes and their electrical properties," *Chemical Physics Letters, Elsevier Science BV*, vol. 427, pp. 107-112, 2006.
27. K. Jiang, W. Liu, L. Wan, and J. Zhang, "Manipulation of ZnO nanostructures using dielectrophoretic effect," *Sensors And Actuators B-Chemical, Elsevier Science SA*, vol. 134, pp. 79-88, 2008.
28. A. Subramanian, B. Vikramaditya, L. Dong, D. Bell, and B. J. Nelson, "Micro and Nanorobotic Assembly Using Dielectrophoresis," *Proceedings of Robotics: Science and Systems*, 2005.

29. X. Chen, T. Saito, H. Yamada, and K. Matsushige, "Aligning single-wall carbon nanotubes with an alternating-current electric field," *Applied Physics Letters, American Inst. Physics*, vol. 78, pp. 3714-3716, 2001.
30. S. Raychaudhuri, S. A. Dayeh, D. Wang, D. and E. T. Yu, "Precise semiconductor nanowire placement through dielectrophoresis," *Nano Letters, American Chemical Soc*, vol. 9, pp. 2260-2266, 2009.
31. V. La Ferrara, B. Alfano, E. Massera, and G. Di Francia, "Single palladium nanowire growth in place assisted by dielectrophoresis and focused ion beam," *Journal of Nanoscience and Nanotechnology*, vol. 9, pp. 2931-2936, 2009.
32. T. H. Kim, C. O. Jang, H. K. Seong, H. J. Choi, and S. K. Lee, "Fabrication and electrical characterization of heterojunction Mn-Doped GaN nanowire diodes on n-Si Substrates (GaN:Mn NW/n-Si)," *Journal of Electronic Materials*, vol. 38, pp. 505-510, 2009.
33. A. Motayed, and A. V. Davydov, "GaN-nanowire/amorphous-Si core-shell heterojunction diodes," *Applied Physics Letters*, vol. 93, 2008.
34. J. W. Lee, K. J. Moon, M. H. Ham, and J. M. Myoung, "Dielectrophoretic assembly of GaN nanowires for UV sensor applications," *Solid State Communications*, vol. 148, pp. 194-198, 2008.
35. A. Motayed, M. He, A. V. Davydov, J. Melngailis, and S. N. Mohammad, "Realization of reliable GaN nanowire transistors utilizing dielectrophoretic alignment technique," *Journal of Applied Physics*, vol. 100, 2006.
36. A. Singh, X. Li, V. Protasenko, G. Galantai, M. Kuno, H. Xing, and D. Jena, "Polarization-sensitive nanowire photodetectors based on solution-synthesized CdSe quantum-wire solids," *Nano Letters*, vol. 7, pp. 2999-3006, 2007.
37. A. Zoy, and A. G. Nassiopoulou, "Growth and electrical characterization of thin conductive Au nanoparticle chains on oxidized Si substrates between electrodes for sensor applications," *Physica Status Solidi A-Applications and Materials Science*, vol. 205, pp. 2621-2624, 2008.
38. L. Dong, J. Bush, V. Chirayos, R. Solanki, and J. Jiao, "Dielectrophoretically controlled fabrication of single-crystal nickel silicide nanowire interconnects," *Nano Letters*, vol. 5, pp. 2112-2115, 2005.

39. W. H. Yeo, F. L. Chou, K. Oh, K. H. Lee, and J. H. Chung, "Hybrid nanofibril assembly using an alternating current electric field and capillary action," *Journal of Nanoscience and Nanotechnology*, vol. 9, pp. 7288-7292, 2009.
40. C. Uran, E. Unal, R. Kizil, and H. V. Demir, "On-chip-integrated nanowire device platform with controllable nanogap for manipulation, capturing, and electrical characterization of nanoparticles," *IEEE Journal of Selected Topics in Quantum Electronics*, vol. 15, pp. 1413-1419, 2009.
41. H. Huang, Y. C. Lee, O. K. Tan, W. Zhou, N. Peng, and Q. Zhang, "High sensitivity SnO₂ single-nanorod sensors for the detection of H₂ gas at low temperature," *Nanotechnology*, vol. 20, 2009.
42. M. Zhao, G. Hu, H. Zhou, K. Zheng, G. Zhu, Y. Cui, and C. Xu, "Dielectrophoretic assembly of ZnO nanowires," *Chinese Optics Letters*, vol. 7, pp. 235-237, 2009.
43. A. Yoon, W. K. Hong, and T. Lee, "Fabrication and characterization of directly-assembled ZnO nanowire field effect transistors with polymer gate dielectrics," *Journal Of Nanoscience And Nanotechnology*, vol. 7, pp. 4101-4105, 2007.
44. C. Lao, J. Liu, P. Gao, L. Zhang, D. Davidovic, R. Tummala, and Z. Wang, "ZnO nanobelt/nanowire Schottky diodes formed by dielectrophoresis alignment across Au electrodes," *Nano Letters*, vol. 6, pp. 263-266, 2006.
45. D. Wang, R. Zhu, Z. Zhou, and X. Ye, "Controlled assembly of zinc oxide nanowires using dielectrophoresis," *Applied Physics Letters*, vol. 90, 2007.
46. D. L. Fan, R. C. Cammarata, and C. L. Chien, "Precision transport and assembling of nanowires in suspension by electric fields," *Applied Physics Letters*, vol. 92, 2008.
47. S. Evoy, N. DiLello, V. Deshpande, A. Narayanan, H. Liu, M. Riegelman, B. Martin, B. Hailer, J. Bradley, W. Weiss, T. Mayer, Y. Gogotsi, H. Bau, T. Mallouk, and S. Raman, "Dielectrophoretic assembly and integration of nanowire devices with functional CMOS operating circuitry," *Microelectronic Engineering, Elsevier Science BV*, vol. 75, pp. 31-42, 2004.
48. S. Kumar, Y.K. Seo, and G. H. Kim, "Manipulation and trapping of semiconducting ZnO nanoparticles into nanogap electrodes by dielectrophoresis technique," *Applied Physics Letters, American Inst. Physics*, vol. 94, 2009.

49. M. S. Kumar, S. H. Lee, T. Y. Kim, T. H. Kim, S. M. Song, J. W. Yang, K. S. Nahm, and E. K. Suh, "DC electric field assisted alignment of carbon nanotubes on metal electrodes," *Solid-State Electronics*, vol. 47, pp.2075-2080, 2003.
50. T. J. Kuo, C. N. Lin, C. L. Kuo, and M. H. Huang, "Growth of ultralong ZnO nanowires on silicon substrates by vapor transport and their use as recyclable photocatalysts," *Chemistry Of Materials, American Chemical Soc.*, vol. 19, pp. 5143-5147, 2007.
51. X. M. Cai, F. Ye, S. Y. Jing, D. P. Zhang, P. Fan, and E. Q. Xie, "A systematic study of chemical vapor deposition growth of InN," *Applied Surface Science, Elsevier Science BV*, vol. 255, pp. 2153-2158, 2008.
52. Y. Heo, D. Norton, L. Tien, Y. Kwon, B. Kang, F. Ren, S. Pearton, and J. LaRoche, "ZnO nanowire growth and devices," *Materials Science and Engineering: R: Reports*, vol. 47, pp. 1-47, 2004.
53. M. Law, J. Goldberger, and P. Yang, "Semiconductor nanowires and nanotubes," *Annual Review of Materials Research*, vol. 34, pp. 83-122, 2004.
54. Y. Yan, L. Zhou, L. Yu, and Y. Zhang, "Morphology evolution of hierarchical ZnO nanostructures modulated by supersaturation and growth temperature," *Applied Physics A-Materials Science & Processing, Springer*, vol. 93, pp. 457-465, 2008.
55. H. Tang, J. C. Chang, Y. Shan, D. D. D. Ma, T. Y. Lui, J. A. Zapien, C. S. Lee, and S. T. Lee, "Growth mechanism of ZnO nanowires via direct Zn evaporation," *Journal Of Materials Science, Springer*, vol. 44, pp. 563-571, 2009.
56. J. Y. Li, and H. Li, "Physical and electrical performance of vapor-solid grown ZnO straight nanowires," *Nanoscale Research Letters, Springer*, vol. 4, pp.165-168, 2009.
57. B. Yao, Y. Chan, and N. Wang, "Formation of ZnO nanostructures by a simple way of thermal evaporation," *Applied Physics Letters, American Inst. Physics*, vol. 81, pp.757-759, 2002.
58. J. B. Baxter and E. S. Aydil, "Metallorganic chemical vapor deposition of ZnO nanowires from zinc acetylacetonate and oxygen," *Journal Of The Electrochemical Society, Electrochemical Soc Inc*, vol. 156, pp. H52-H58, 2009.

59. J. P. Kar, M. H. Ham, S. W. Lee, and J. M. Myoung, "Fabrication of ZnO nanostructures of various dimensions using patterned substrates," *Applied Surface Science, Elsevier Science BV*, vol. 255, pp. 4087-4092, 2009.
60. B. Wen, Y. Huang, and J. J. Boland, "Controllable growth of ZnO nanostructures by a simple solvothermal process," *Journal Of Physical Chemistry C, American Chemical Soc.*, vol. 112, pp. 106-111, 2008.
61. C. Pan and J. Zhu, "The syntheses, properties and applications of Si, ZnO, metal, and heterojunction nanowires," *Journal Of Materials Chemistry, Royal Soc. Chemistry*, vol.19, pp.869-884, 2009.
62. H. A. Pohl, "Dielectrophoresis: the behavior of neutral matter in nonuniform electric fields," *Cambridge University Press*, 1978.
63. S. Murali, V. Ng, C. C. Huang, and J. Conley, 2010. Unpublished Research.
64. F. Fang, D. Zhao, J. Zhang, D. Shen, Y. Lu, X. Fan, B. Li, and X. Wang, "The influence of growth temperature on ZnO nanowires," *Materials Letters*, vol. 62, pp. 1092-1095, 2008.
65. Y. H. Kang, C. G. Choi, Y. S. Kim, and J. K. Kim, "Influence of seed layers on the vertical growth of ZnO nanowires," *Materials Letters, Elsevier Science BV*, vol. 63, pp. 679-682, 2009.
66. M. Huang, Y. Wu, H. Feick, N. Tran, E. Weber, and P. Yang, "Catalytic growth of zinc oxide nanowires by vapor transport," *Advanced Materials, Wiley-VCH Verlag GMBH*, vol. 13, pp.113-116, 2001.
67. D. S. Kim, U. Goesele, and M. Zacharias, "Surface-diffusion induced growth of ZnO nanowires," *Journal Of Crystal Growth, Elsevier Science BV*, vol. 311, pp. 3216-3219, 2009.
68. J. F. Conley, Jr., L. Stecker, and Y. Ono, "Directed assembly of ZnO nanowires on a Si substrate without a metal catalyst using a patterned ZnO seed layer," *Nanotechnology*, vol. 16, pp. 292-296, 2005.
69. L. J. Brillson and Y. Lu, *Surface Properties and Electrical Contacts on ZnO, ZnO Materials for Electronic and Optoelectronic Device Applications*, Ch. V, eds. C. W. Litton, D. C. Litton, and T. C. Collins, John Wiley & Sons, Ltd., London, UK, 2009.

70. J.Triska, Graduate student, Materials and Devices, EECS, Oregon State University, 2010.

APPENDICES

A. Additional Images of Nanowire Removal


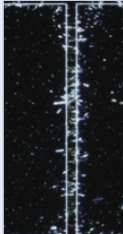
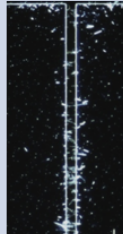
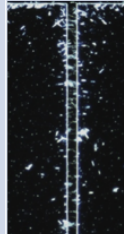
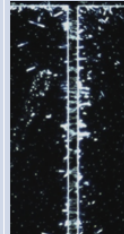
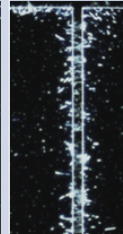
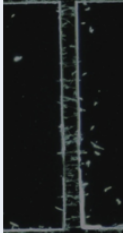



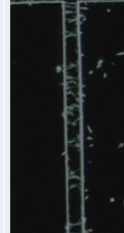
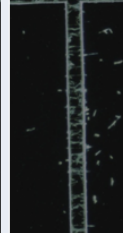






A.1 Align at 1 kHz, IPA Flush at 1 kHz – 100 kHz, and 1 kHz-200 kHz

The following images show that with frequency tuning and IPA flushing, excess nanowires that are trapped at the edges of the electrodes can be removed. The results on alignment at 1 kHz, flushing with IPA at 1 kHz-100 kHz and at 1 kHz-200 kHz were taken from three different devices. However, the images represent the same location on each device.

	0.2mm 1	0.2mm 2	0.5mm 1	0.5mm 2	0.8mm 1	0.8mm 2	Average Angle
Align @ 1 kHz							~10 deg
Flush @ 1 kHz, 100 kHz							~6 deg
Flush @ 1 kHz, 200 kHz							~6 deg

A.2 Align at 1 kHz, IPA Flush at 1 kHz – 100 kHz, and 1 kHz-1 MHz

The results on alignment at 1 kHz, flushing with IPA at 1 kHz-100 kHz and at 1 kHz-1 MHz were taken from three different devices. However, the images represent the same location on each device.

	0.2mm 1	0.2mm 2	0.5mm 1	0.5mm 2	0.8mm 1	0.8mm 2	Average Angle
Align @ 1 kHz							~10 deg
Flush @ 1 kHz, 100 kHz							~6 deg
Flush @ 1 kHz, 1 MHz							~5 deg

